

**Novel Micro System for Accelerated Determination of Diffusion Coefficient**

by

Kirn Augusta Cramer

A thesis submitted to the Graduate Faculty of  
Auburn University  
in partial fulfillment of the  
requirements for the Degree of  
Master of Science

Auburn, Alabama  
December 8, 2012

Keywords: Micro System, Micro mixer, Diffusion, Taylor Dispersion

Copyright 2012 by Kirn Augusta Cramer

Approved by

Jong Wook Hong, Chair, Associate Professor of Materials Engineering  
Jeffrey W. Fergus, Professor of Materials Engineering  
Barton C. Prorok, Associate Professor of Materials Engineering

## Abstract

Diffusion plays a paramount role in many scientific areas. In the scientific field, the term diffusion coefficient,  $D$ , is generally used as the parameter for quantifying the diffusion phenomena. At present, diaphragm cell, chromatography or optical based methods are commonly employed to determine the  $D$  value of various solutions. However, these methods have major disadvantages; they use bulky equipment and require a lengthy experimental time. In the past, to overcome these disadvantages, many research groups have tried to reduce the size of the instrument, as well as decrease the performance time, by using microfluidic-based devices. This study will address the problem of achieving quick quantification of diffusion coefficients by using a novel micro system fluidic device. The major advantages of this device include minimum sample and device size, short experimental testing time, and user-friendly programming allowing for acceleration of determining a diffusion coefficient.

## Acknowledgments

The author would like to acknowledge her most sincere appreciation towards her advisor Dr. Jong Wook Hong, for his continued encouragement, support, enthusiasm and guidance. The author is deeply thankful to her committee members, Dr. Jeffrey W. Fergus, and Dr. Bart Prorok, for their valuable support, teachings and assistance during the course of this study. The author would like to also thank Mr. Charles Ellis, Mr. Shakib Morshed and Mrs. Tamara Isaacs-Smith of Alabama Microelectronics Science and Technology Center (AMSTC) for permission and assistance in using the clean room for microfabrication.

The author would like to express her deep gratitude and gratefulness to Mr. Chance Tara, Mr. Sachin Jambovane, Mr. Hoon Suk Rho and Dr. Morgan Hamon, for passing on their knowledge and assistance during the course of these projects. The author would like to also share her warmest appreciation for Mr. Chance Tara for his invaluable MATLAB programming assistance and Mr. Sachin Jambovane for providing the theoretical Fourier concentration profile equation. The author would like to thank the following individuals for their assistance and collaboration on various projects: Dr. Jeyhoon Khodadadi, Mr. Mahmoud Sedeh, Mr. Cihan Uzunpinar, and Dr. Maria Auad. The author would also like to thank the company of her current and past research group members: Dr. Morgan Hamon, Dr. Woon Seob Lee, Dr. Jae Young Yun, Mr. Sachin Jambovane, Mr. Hoon Suk Rho, Mr. Jing Dai, Miss Tina Chen, Mr. Austin Adamson, Mr. Chance Tara, Miss Lauren

Bradley, Mr. Xiaoyun Yang, Miss Jing Zou, Miss Hye Young Sim, Mr. Ryan Khodadadi, Miss Oxana Katalevskaya, Mr. Samuel Thompson, and Mr. Andy Hanna.

The author would also like to thank to her family and friends, Joyce, Al, Anna, Kam, and JJ Cramer, Sam Raymond, Emily and Ty Stafford, Steve Moore and Christen May, for their continuous love, support, encouragement and patience.

## Table of Contents

Abstract .....	ii
Acknowledgments .....	iii
List of Tables .....	viii
List of Figures .....	ix
List of Abbreviations .....	x
Chapter 1 Introduction .....	1
1.1 Background .....	1
1.2 Microfluidic platform .....	2
1.3 Multilayer soft lithography .....	3
1.4 Pneumatic control systems .....	7
1.4.1 Pneumatic valves .....	7
1.4.2 Pneumatic mixer .....	9
1.5 Diffusion study on a chip .....	12
1.6 Scope of the study .....	16
Chapter 2 Literature review .....	17
2.1 Introduction .....	17
2.2 Conventional methods .....	18
2.3 Segmented flow microfluidic systems .....	22
2.4 Static and dynamic microfluidic systems .....	23

2.5	Refractive index gradient detected microfluidic systems .....	24
2.6	Summary .....	25
Chapter 3	Development of the diffusion chip .....	26
3.1	Introduction .....	26
3.2	Device design .....	27
3.2.1	Diffusion chip design version I .....	30
3.2.2	Diffusion chip design version II .....	33
3.2.3	Diffusion chip design version III .....	37
3.3	Mold fabrication .....	42
3.4	Chip fabrication .....	45
3.5	Experimental setup and operation .....	53
3.6	Results and discussion .....	57
3.6.1	Introduction .....	57
3.6.2	Equation validation .....	58
3.6.3	Data analysis .....	63
3.6.4	SPSS analysis .....	64
3.6.5	MATLAB analysis .....	67
3.7	Conclusions .....	69
Chapter 4	Summary and conclusions.....	71
4.1	Conclusions of the research .....	71
References	.....	72
Appendix I	MatLab Code .....	75

## List of Tables

Table 3.1 Soft lithography chip making procedures .....	46
Table 3.2 SPSS regression analysis results.....	66

## List of Figures

Figure 1.1 Chemical structure of silicone rubber or polydimethylsiloxane.....	5
Figure 1.2 Cross-sectional view of the process flow for multilayer soft lithography.....	6
Figure 1.3 Cross-sectional schematic of a valve closing .....	7
Figure 1.4 Diagram of valve closing for rectangular and rounded channels. The dotted lines show the contour of the PDMS membrane as pressure is increased. ....	9
Figure 1.5 Sequence of valve operation of pneumatically operated peristaltic micro mixer inducing fluidic flow .....	10
Figure 1.6 Schematic of working of a pneumatically operated peristaltic micro mixer ....	11
Figure 1.7 Schematic of rotary pump and appropriate variable labeling.....	11
Figure 1.8 Basic principles of diffusion.....	13
Figure 1.9 Schematic of Taylor dispersion of long tube related to a closed tube chamber on a microfluidic system.....	15
Figure 2.1 Simple diaphragm cell, a Northrop-Anson cell.....	19
Figure 2.2 Apparatus presented by Taylor used for observing dispersion in a tube.....	21
Figure 2.3 Sample dispersion study device using piezoelectric bending disc actuator and fiber optic detection .....	23
Figure 3.1 Cup and cone progression model .....	27
Figure 3.2 Basic design with detail of a reaction chamber and valve close/open key.....	30
Figure 3.3 Chip design version I.....	31
Figure 3.4 Concentration versus time data corresponding to the ROI within reaction chamber. The green line indicates the release of the center valve, thus the start of the experiment and the blue line indicates 4 seconds later. ....	33



Figure 3.5 Chip design version II .....	34
Figure 3.6 Device fabricated of design version II. No evidence of channel collapsing but shut off valves for reagent metering interferes with reagent flow .....	35
Figure 3.7 Device fabricated of design version II. Center valve with 28 psi pressure shutting valve with reaction chamber filled with air from chip fabrication .....	36
Figure 3.8 Chip design version III .....	37
Figure 3.9 A fabricated chip of design version III of a good chip.....	38
Figure 3.10 Device fabricated of design version III. Center valve pressure not disengaging properly affecting fluid flow drastically. 50.922 seconds after releasing the center valve.....	40
Figure 3.11 Chip design progression – reaction chamber detail view, version I (a), version II (b), and version III (c) .....	41
Figure 3.12 Schematic of mold fabrication process.....	47
Figure 3.13 Microfluidic chip made of design III filled with food dye for visualization of structure, connected to Tygon tubing and includes a quarter for size comparison	53
Figure 3.14 Schematic of experimental setup.....	54
Figure 3.15 Schematic of experimental operational procedures.....	55
Figure 3.16 MATLAB plot of theoretical concentration versus time profile give the Fourier concentration profile and experimental and known values.....	60
Figure 3.17 Concentration versus time profile of two experiments at 5Hz, standard mixing sequence of water and dye.....	62
Figure 3.18 Average peak and valley points from test 1, 2 and 3 from Figure 3.17 .....	63
Figure 3.19 SPSS regression analysis curves for the average peaks .....	65
Figure 3.20 SPSS regression analysis curves for the average valleys .....	66
Figure 3.21 MATLAB output results of the peak value analysis of water and dye .....	68
Figure 3.22 MATLAB plot of the peak value analysis of water and dye .....	69

## List of Abbreviations

CE	Capillary/microchannel electrophoresis
LOC	Lab on a chip
PCR	Polymerase chain reaction
PDMS	Polydimethylsiloxane
MEMS	Micro electro mechanical systems
DRIE	Deep reactive ion etching
SFB	Surface fusion bonding
ECR	Electron cyclotron resonance
CTMS	Chlorotrymethylsilate
$\mu$ TAS	Micro total analysis system
AMSTC	Alabama Microelectronics Science and Technology Center
DPI	Dots per inch
ROI	Region of interest
SPSS	Statistical Package for the Social Sciences
NMR	Nuclear magnetic resonance

## **Chapter 1**

### **Introduction**

#### **1.1 Background**

Microfluidic systems allow for the study of the behavior and response of controlled fluidics within a confined, by design, system. For a definition the following will be used: microfluidics is the science and technology of systems that process or manipulate small ( $10^{-9}$  to  $10^{-18}$  liters) amounts of fluids, using channels with dimensions of tens to hundreds of micrometers.[1] It is possible to scale down a complicated system to a microfluidic system. By doing so, microfluidic systems use minimum sample volumes, can precisely meter samples, and can achieve quick response and experiment times. All these things considered increase the throughput of a microfluidic system experimentally compared to many of its predecessor techniques.

The field of microfluidics is a multidisciplinary field including chemical engineering, biological studies, physics, civil and materials engineering, to name a few. It also includes the ever growing study of biological interactions with drug candidates. Continuing advances in micro fluidic devices has opened the door to innovative micro scale analysis allowing technical barriers to be left by the wayside. Diffusion is the process by which matter is transported from one part of a system to another as a result of random molecular motions.[2] The ability to quickly and accurately measure diffusion coefficients is important to assessing and interpreting the quality of experimental results obtained from liquid chromatography and capillary/microchannel electrophoresis

(CE).[3] This information can be valuable in drug, biological and other applications. By using a microfluidic system to determine diffusion coefficient, experimental times and sample size are significantly smaller compared to conventional methods, yet still as accurate.

## **1.2 Microfluidic platform**

Microfluidics belongs to an area of study called micro total analysis systems ( $\mu$ TAS), also called “lab on a chip” (LOC). Within the  $\mu$ TAS or LOC, the goal is to house the full testing system within a single device. This field crosses a variety of disciplines including chemistry, biology, bioengineering, physics, electronics, clinical/medical science, chemical engineering and materials science. It has been able to grow due to advances in semiconductors and micro electro mechanical systems (MEMS). As these systems are at the forefront of technology, it seems only appropriate that chemical screening and analysis should also advance by miniaturization, resulting in faster response time and automated sample handling.

The field of microfluidics or  $\mu$ TAS has grown rapidly since its beginnings in the early 1990s. The very beginning can be traced back over 35 years to the development of a the first analytical miniaturized device, a gas chromatographic analyzer, fabricated on silicon chip base.[4, 5] Despite its rapid separation capabilities and minute size, the response within the scientific community to this first silicon chip device was almost nonexistent, most likely due to the lack of technological experience dealing with this type of device.[6] Despite the low effects at the time, between 1990 and 1993 there was an emergence of advances and studies performed in the  $\mu$ TAS field. During this time, Manz

and colleagues presented a novel miniaturized open-tubular liquid chromatography on a silicon wafer[7] and presented the concept of “miniaturized total chemical analysis system”. [8] These advances led to others studying and making exciting developments in micropump systems[9, 10], sample injector systems[11, 12] and even the use of microfabricated chambers to carry out DNA amplification, also known as Polymerase chain reaction (PCR).[6, 13] Since then many researchers have used microfluidics for numerous studies, utilizing different elemental systematic tools possible by the advances within the fabrication techniques. New methods of fabrication systems and of systematic components have become essential elements of microchemical ‘factories’ on a chip.[1] Such systematic components include microchannels that serve as pipes, and other structures that form valves[14, 15], mixers[16-18] and pumps.

### **1.3 Multilayer soft lithography**

These micro systems are designed to have all three dimensions of the structure on the microscale, producing fluid volumes in the nanoliter or picoliter scale. There are various methods of producing these systems. When talking on a small scale such as micro and nanometer, we must consider the fabrication method. Microcontact printing creates the pattern of the structure out of self-assembled monolayers (SAMs) on the submicrometer scale as a viable method.[19] There are also many micromachining methods for creating microstructures including deep reactive ion etching (DRIE)[20] and surface fusion bonding (SFB) and electron cyclotron resonance (ECR) source to produce high-aspect-ratio narrow-gap silicon devices.[6] Another method is microtransfer molding, in which a large areas of micrometer scale structures can be created by filling

microchannels of an elastomeric mold with precursor, curing the precursor, and then removing the mold to reveal a system of micro structures.[21]

Soft lithography is a low-cost technique for microfluidic devices led the way by Whiteside, Xia and Zhao from Harvard University.[22] This method allows for rapid prototyping (it does not need a clean room for fabrication) and requires simple equipment for fabrication. Easy fabrication methods allow users with basic, high school scientific laboratory experience to be able to create reproducible, complex micro systems. Soft lithography uses soft, organic materials such as polymeric materials to create microstructure patterns from negative patterned molds. By using a single elastomer material such as polydimethylsiloxane (PDMS), these microstructure patterns can be visible, allowing for countless number of studies that can be performed. PDMS has become the polymer of choice for soft lithography fabrication, as it has great optical transparency and is a very flexible polymer, and therefore can be manipulated easily and has good biocompatibility.[23]

PDMS is produced by GE Silicones and Momentive Performance Materials as a two-component silicon rubber, RTV 615 (room temperature vulcanizing), also known as silicone RTV. The two components come as a kit of the two solutions by a 10:1 weight ratio. Component A contains the PDMS monomer, while component B is a cross linking agent. When mixed at a 10:1 ratio (A:B, respectively) the compound can cure, according to GE Silicones technical data sheet of RTV 615, in either 1 hour at 100°C or 15 minutes at 150°C, insuring that the compound will be cure within 24 hours at 25°C. Figure 1.1 shows the chemical structure of PDMS [24], while equation 1.1 shows the reaction mechanism of covalent bonding in two component addition-cure PDMS.

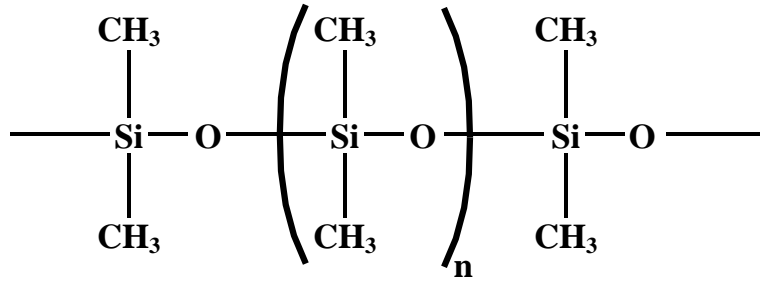
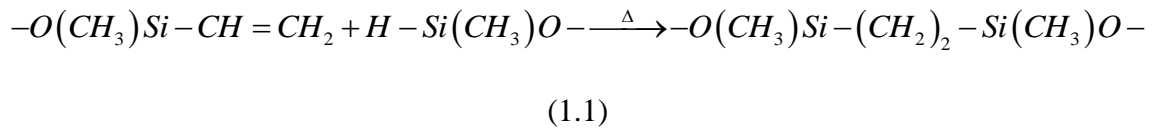


Figure 1.1 Chemical structure of silicone rubber or polydimethylsiloxane.

**Source:** [(Callister 2003)]



By decreasing the ratio of cross-linking agent, the resulting PDMS has an increase in flexibility. We are then able to produce various layers of PDMS at different ratios. Multilayer soft lithography (MSL) combines the principles of soft lithography fabrication, as introduced by Whiteside, Xia and Zhao, and the flexibility of various ratios of PDMS to create multiple layers of microstructures within PDMS and bond the layers together. Figure 1.2 shows a cross-sectional representation of the fabrication process flow of a MSL. The top layer, as seen on the left, is first cured onto the mold then removed and bonded to the cured layer on the second mold. The final system can be removed from the bottom mold and bonded to a substrate, glass slide, and operated.

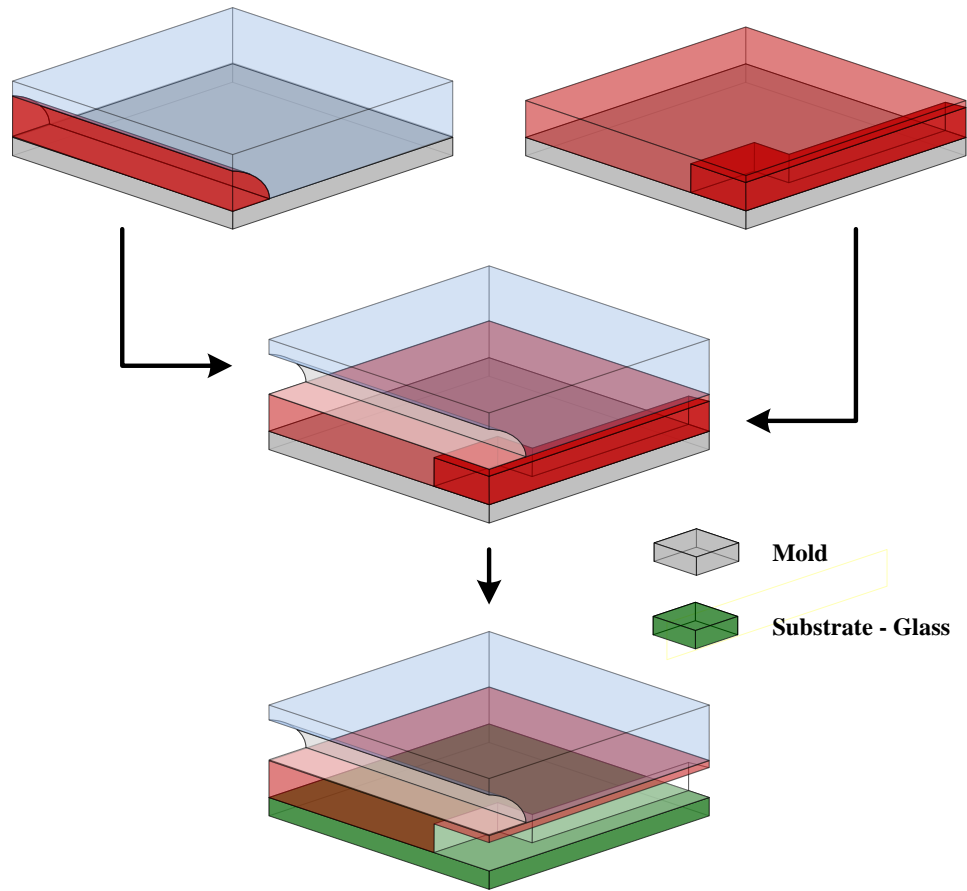


Figure 1.2 Cross-sectional view of the process flow for multilayer soft lithography.

**Source:** [(Unger et al. 2000)]

With the introduction of multilayer soft lithography by Unger et al.[25] in 2000, this technique for creating and manipulating microstructures has expanded the possibilities of applications in microfluidics. This allows scientists to design microfluidic devices even more similar to the *in vivo* subjects than before. This gives great potential for advances to be made within the biotechnology field.



## 1.4 Pneumatic control systems

### 1.4.1 Pneumatic valves

With the introduction of the MSL by Unger et al.[25] the interaction between two overlapping microchannels can be studied. By designing for different layers' microchannels to overlap at certain locations, we can create areas of interaction. This allows structures such as on-off valves, switching valves, and pumps to be produced within the the PDMS structure. There are two types of valve orientations; the control layer containing the valves can either be above or below the fluidic layer that is to have the fluid flow controlled. Figure 1.3 illustrates a cross-sectional view valve shutting off a control valve below the fluidic microchannel layer.

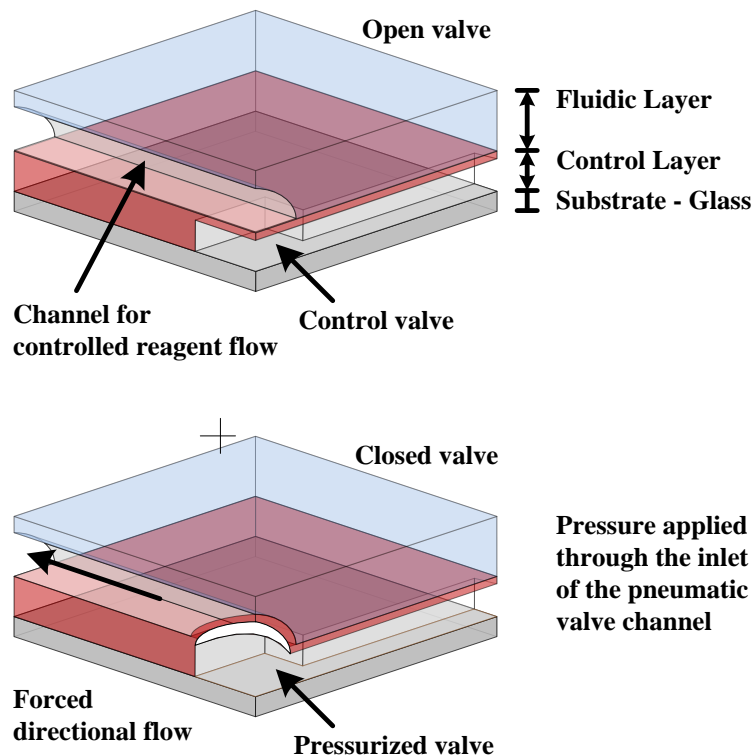


Figure 1.3 Cross-sectional schematic of a valve closing.

Source: [(Unger et al. 2000)]

If the control valve is above the fluidic, then pressure is needed to push down on the membrane of PDMS between the two layers. Generally, the microchannels are 100  $\mu\text{m}$  wide and 10-15 $\mu\text{m}$  high, allowing for a 100  $\mu\text{m}$  x 100  $\mu\text{m}$  interaction area. The amount of pressure needed to push down on the membrane depends on the membrane thickness. Fabrication methods can control the membrane thickness, usually needing about 30  $\mu\text{m}$  with the previous mentioned dimensions.

With the control layer below and a glass substrate below the control layer, this decreases the response time to activation, which can be critical depending on the device. The shape of the flow channel can also affect the valve performance. The channel cross sections and heights are a result of the mold fabrication process. Unger et al.[25] discussed three different shapes of the fluidic channel: rectangular, trapezoidal and rounded. A rectangular or trapezoidal shaped channel requires more pressure to cause the membrane to touch the roof of the channel than a rounded channel requires. Still, rectangular and trapezoidal channels will not fully close when the membrane is being pushed down due to the corners of the walls. Channels with a rounded cross section above a control valve close completely because as the pressure is applied, the force transfers to the membrane from the edges to the center, resulting in a complete closure. Figure 1.4 demonstrates the difference between pushing up (b) and pushing down (a) similar as that suggested by Unger et al. [25] in 2000. Also, we can see the difference of the contour of the PDMS membrane as pressure is applied to a rectangular cross section (a) and a rounded cross section (b).

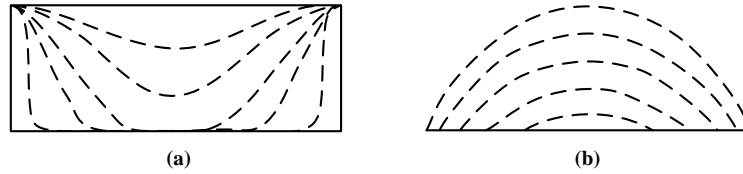


Figure 1.4 Diagram of valve closing for rectangular and rounded channels. The dotted lines show the contour of the PDMS membrane as pressure is increased.

**Source:** [(Unger et al. 2000)]

### 1.4.2 Pneumatic mixer

To realize the full potential of micro systems enabling a full LOC in microfluidics, some obstacles must be overcome. In micro systems, due to the small channel dimensions, reagents observe low Reynolds numbers. Laminar flow occurs at low Reynolds numbers. In laminar flow, mixing of fluids is mainly done by diffusion, which is good for our study, however mixing can be very slow. To improve the mixing time of reagents, sequential control of pneumatic valves can induce flow. Such flow was first studied by Chou, Unger and Quake in 2001 as a microfabricated rotary pump.[26] By operating valves in series of a closed loop, the valves can function as a peristaltic pump. A peristaltic pump, or roller pump, is a positive displacement pump that pushes fluids through flexible tubing as rollers apply pressure to the fluids and rotate, thus moving the fluid in the direction of the rollers rotation. To realize this on a micro system device, at least three pneumatic valves are placed in series and operated sequentially, thus creating directional flow. Figure 1.5 shows a three-step sequence of pneumatically operated peristaltic micro valves inducing fluidic flow.

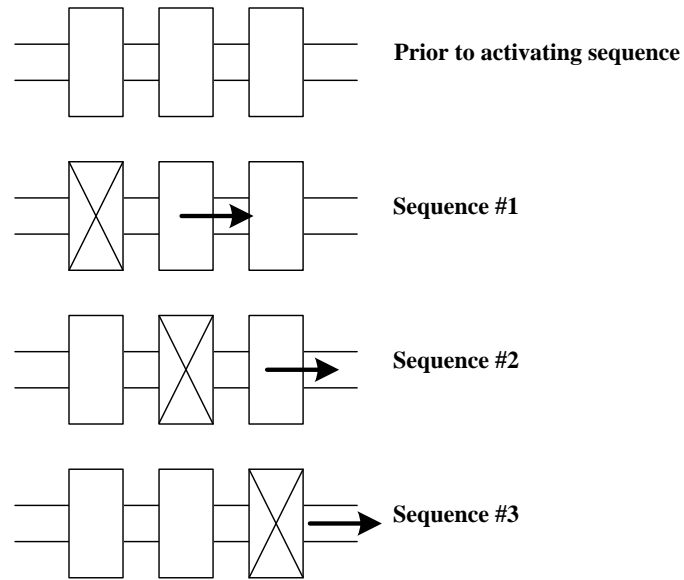


Figure 1.5 Sequence of valve operation of pneumatically operated peristaltic micro mixer inducing fluidic flow. **Source:** [(Chou et al. 2001)]

When a peristaltic pump operates in a loop, an active mixer is created. Thus, if we design at least three pneumatic valves in series of a closed loop and operated sequentially. We create flow and the interfaces between the fluids will be stretched which improves mixing. To have well developed and steady flow it is important to have even spacing of the valves. Figure 1.6 shows a schematic of working of a pneumatically operated peristaltic micro mixer with 60° valve separation.

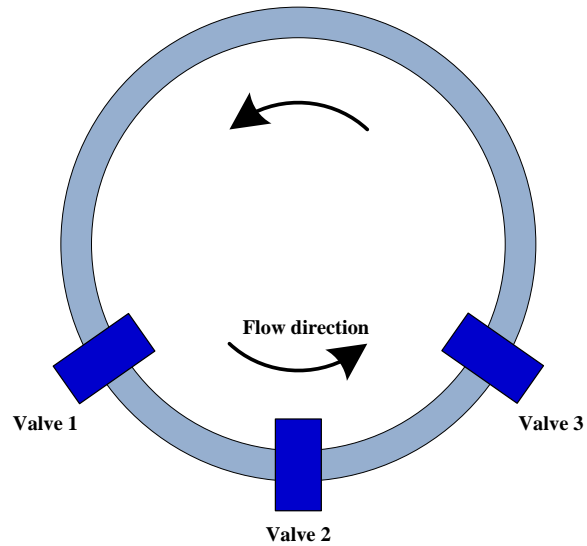


Figure 1.6 Schematic of working of a pneumatically operated peristaltic micro mixer.

**Source:** [(Chou et al. 2001)]

Along with valve degree separation, other design parameters are important to determine the working functions of the micromixer. Figure 1.7 shows the outline of a rotary pump necessary for determining the working function of the pump, such as velocity.

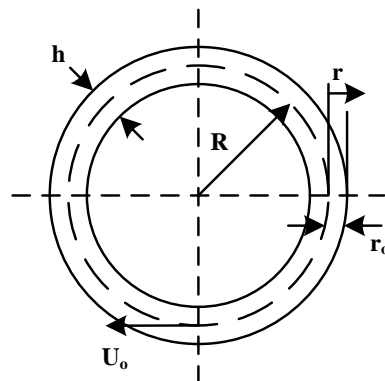


Figure 1.7 Schematic of rotary pump and appropriate variable labeling.

**Source:** [(Chou et al. 2001)]

Equation 1.2 shows how the angular velocity can be calculated according to the designed rotary pump.

$$\omega_o = \frac{U_o}{R} \left( 1 - \left( \frac{r}{r_o} \right)^2 \right) \quad (1.2)$$

Equation 1.2 can be used to determine the angular velocity as  $U_o$  is the maximum velocity at the center of the channel,  $r_o$  is half the width of the channel and  $R$  is the radius of the ring. The mixing time in the microchannel closed loop is directly proportional to the linear velocity of the fluid inside the microchannel.

## 1.5 Diffusion study on a chip

Diffusion is the transport process in which the concentration gradient over distance of one solute affects the flux of a second solute.[27] The diffusion coefficient,  $D$  is the constant at which a unit concentration gradient spreads out over an area per unit of time, standard unit  $m^2/s$ . Figure 1.8 illustrates how two solutions, initially separated (a), will over time diffuse into one another (c) and how each solutions' flux will change as the concentration changes (b) and (d).

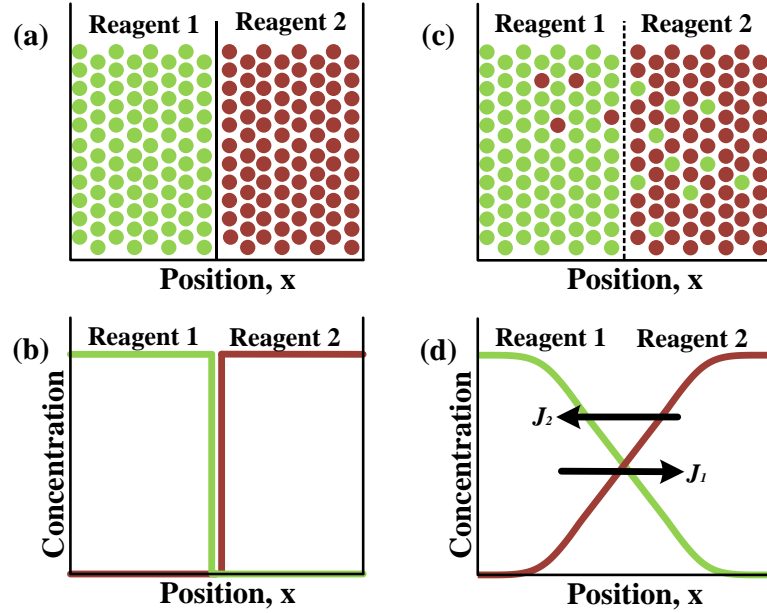


Figure 1.8 Basic principles of diffusion. **Source:** [(Callister 2003)]

When concentration, location and time are all considered Fick's second law of diffusion explains their relationship to one another. According to Fick the change in concentration  $c$  per change in time  $t$  is proportional to the diffusion coefficient  $D$  multiplied by the change in concentration  $c$  per change in length,  $x$ .

$$\frac{\partial c}{\partial t} = -D \frac{\partial^2 c}{\partial x^2} \quad (1.3)$$

Understanding the nature of diffusion is a key advantage to the progress of multi-reagent microfluidic systems. With a known diffusion coefficient, minimal efforts are needed to determine proper concentration ratios and other parameters for applications such as sample analysis, medium preparation and material synthesis. Much investigation has gone into segmented flow of reagents to determine diffusion coefficient.[28]

Segmented flow looks at how concentrations of solvent, sectioned by gas, leaves a film of solution within the channel walls. This film diffuses into passing solvent and is explained by intra diffusion coefficient. Intra diffusion is useful in studying how different concentrations of one solution diffuse into themselves, but is not as useful in the study of multiple liquid reagents. With rectangular observation channels, films of solvent tend to collect at the walls and corners of the channel, thus altering the observed diffusion coefficient. To circumvent this experience of films remaining on the walls, our device utilizes semicircle shaped walls created by a baking process after a master mold is fabricated. This minimizes the effects of sharp edges within the testing chamber, which allow the formation of film deposits. While there are many different experimental methods to determine diffusion coefficients, the diaphragm cell is one of the most basic in principle. A diaphragm cell can be used for diffusion coefficient measurements in which the device initially separates two reagents or two different concentrations. The concentration gradient with respect to time is evaluated to calculate the diffusion coefficient. While this method is theoretically simple, it can utilize hundreds of milliliters of reagents, it is time consuming, and requires certain amount of skills to perform the experiment properly to produce precise measurements.[29]

We can rearrange Taylor dispersion, one of the principals of diffusion, to determine diffusion coefficients in an economical and timely manner. Taylor dispersion is the chromatography method of observing the diffusion of one solution into another. This technique uses a pulse of dye solution injected into a slow stream of solvent within a narrow tube. The observation of the color moving along the tube as a symmetrical column of slowly increasing length allows one to determine the diffusion coefficient



given the concentration change, distance traveled and time lapse. By transforming the long, undisturbed tube from the Taylor dispersion theory into one continuous circular tube, the study of diffusion of a length of tube can be related to the diffusion over time and rotations around the circular tube. When two reagents are initially separated and allowed to diffuse into each other, the phenomenon relies on fluidic pressures and reagents' relative diffusion coefficient. Using microfluidic valves, a three step sequential operation will force the reagents to travel within the enclosed chamber in a hydrodynamic nature. Upon fluidic interface of two reagents, unless the two are immiscible of each other, the reagents will diffuse into one another due to low interfacial tension between the two reagents.[28] By making the chamber circular, the turbulent flow, induced by forces on the reagent, is converted into laminar flow allowing the dispersion theory to take effect. Microfluidic valves induce laminar flow within the compact device, enabling Taylor dispersion theory to be applied to a smaller testing area.

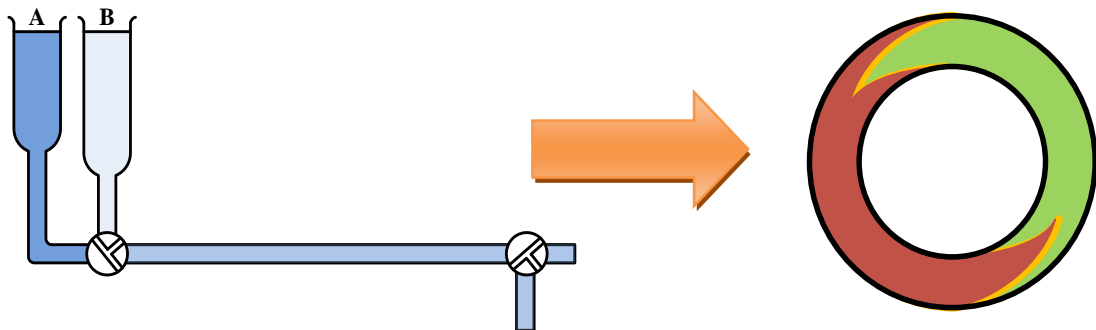


Figure 1.9 Schematic of Taylor dispersion of long tube related to a closed tube chamber on a microfluidic system. **Source:** left drawing[(Taylor 1954)]

## **1.6 Scope of the study**

The focus of this study is to design and evaluate a micro system device that is capable of being a tool to determine, optically, the diffusion coefficient of the two solutions. The integrated microfluidic device will allow reagents to be handled, metered, mixed and optically evaluated. Through this study, various designs are considered, evaluated and compared. Review of previous researchers' studies and mathematical models are studied and reviewed. Details pertaining to data analysis and handling are presented. Discussion of results and further study are presented.

This device is a novel approach to determining a diffusion coefficient using a micro system and has many advantages over conventional and other microfluidic systems. The advantages include a very low sample amount (less than 10 picoliters, per reagent) and experiments are quick, generally less than 5 minutes. The device is also reusable; washing and drying of the system allows for repeatable experiments.

## Chapter 2

### Literature Review

#### 2.1 Introduction

As discussed previously, the definition for diffusion which will be utilized in this study is the transport process in which the concentration gradient over distance of one solute affects the flux of a second solute.[27] Diffusion can also be described as the diffusion of one liquid into another, a solid into a liquid or the transfer of heat or electricity from one system to another.[29] All four examples of transfer involve flow of materials from one or both systems to another creating gradients of concentration, heat or current. The correlation between heat flow and diffusion was first presented by Berthollet in 1803 in his book entitled (roughly translated from French to English) Testing of Static Chemical. [30] Berthollet describes the mechanism of dissolution of a salt crystal into water. Fourier in his 1827 work on theory of heat flow presents that heat flow is a linear function of the temperature gradient.[31] In 1855 Fick developed what is now known as his second law of diffusion, equation 1.3.[32] The force responsible for diffusional flow is the gradient of concentration. With Fick's evaluation of Fourier's treatment of heat conduction problem, he simply replaced the temperature gradient in Fourier's equation by the concentration gradient,[29] thus allowing us to use equations for heat flow and relate them to concentration flow and diffusion. In Crank's second addition of The Mathematics of Diffusion[2] he explains in detail how conversion of heat flow to diffusion solutions can be done given Fick's second equation and the theory

of heat flow. Looking at Fick's second law, equation 1.3, we see the flux of the system is proportional to the concentration gradient multiplied by the diffusion coefficient. The diffusion coefficient,  $D$  is the constant at which a unit concentration gradient spreads out over an area per unit of time, standard unit  $m^2/s$ . Since the time of Berthollet, Fourier and Fick all answers on diffusion have not been obtained as we are still interested in the movement of concentrations across systems. This can be accomplished this quantitatively by comparing diffusion coefficients. How to determine the diffusion coefficient must be known. As technology and our knowledge of diffusion has advanced, so have conventional experimental methods. In this chapter, conventional experimental methods will be discussed, compared with one another and micro system methods for determining diffusion coefficient.

## **2.2 Conventional methods**

The effects of mixing due to thermal and mechanical disturbances are difficult to factor out when studying concentration flow due to diffusion. However, in very narrow diffusion columns with capillaries, these unwanted effects, such as thermal and mechanical, are minimal. Methods of this nature were considered steady-state methods.

Northrop and Anson[33] introduced the diaphragm cell method in 1929, in which a diluted solution and a concentrated solution are separated by a glass capillary, with the diluted solution on top in a diaphragm, usually maintained horizontally. Diffusion was allowed to occur above and below and was assumed to be linear and by natural convection. Many adjustments were possible, including adding stirrers and different materials for dividing capillary and cell containers. Diaphragm cell has the advantages of

simplicity, low cost, and, when used correctly, precision. However, the experiments are usually time-consuming, approximately 24 hours for one experiment and reagent consuming, and the smallest volume mentioned was 33 mL per solution. Another disadvantage is that for calibration, the apparatus must be tested with a system of known diffusivity. Figure 2.1 shows the simplest of diaphragm cells, a Northrop-Anson cell.

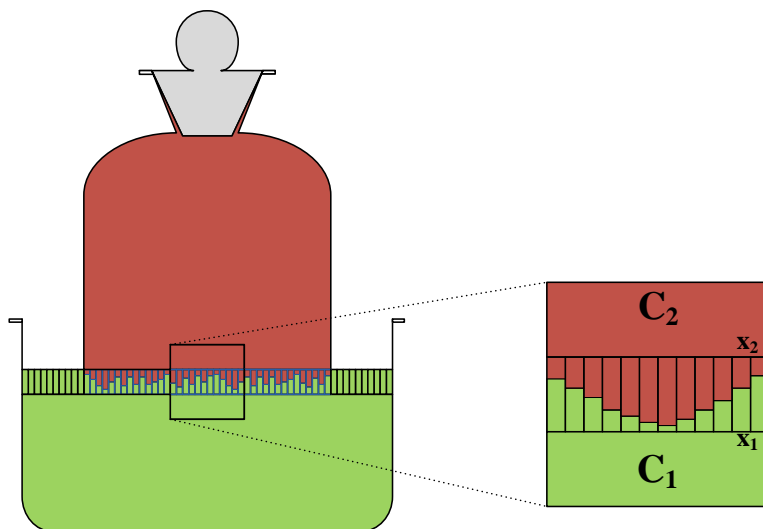


Figure 2.1 Simple diaphragm cell, a Northrop-Anson cell. **Source:** [(Tyrrell 1984)]

Graham[34] introduced ‘layer analysis’ in 1861 for restricted diffusion analysis. For this method, a concentrated solution is introduced below a column of a less concentrated solution in a tall narrow container. The solutions are allowed to diffuse completely, then the column is separated into even layers and analyzed separately.

Another optical technique studies how a beam of light passes through a diffusion column and the resulting bend of the beam. The bend angle is proportional to the refractive index gradient, and if the diffusion boundary is symmetrical can produce a time-dependent pattern. Such pattern is parallel to the angle of the beam introduced to

the diffusion column and shows the interference in fringes. These fringes are called Gouy fringes and the diffusion coefficient can be obtained from the pattern of the fringes produced. In 1879 Louis Georges Gouy first showed the broadened slit image consisting of bands, alternating from light to dark.[35], thus the fringes earned their name. Another optical method is the study of Rayleigh fringes, which are similar to Gouy fringes in experimental setup and results. However, Rayleigh fringes are produced by a double slit in the vertical direction of the light while Gouy has a single slit. While precise optical studies of interdiffusion have been conducted, with both Gouy and Rayleigh interferometers both producing fringe patterns,[29] these systems can be costly and proper setup can be time consuming.

Electrochemical methods for diffusion coefficient determination involve electroactive materials and electrode surface interaction. Diffusion coefficients of electroactive species can be measured, given the electroactive species present in a solution contain a large excess of a backing electrolyte whose ions are not themselves electroactive.[29] The rate of migration towards an electrode surface can be determined only by diffusion and is governed by Fick's law. An exact analysis in this method is difficult, and this method can only be used for electroactive materials and thus is not ideal for a baseline diffusion method to be used for many solution combinations.

Nuclear magnetic resonance (NMR) spin-echo technique has advantages over other techniques because it is capable of measuring diffusion coefficients over several orders of magnitude and requires small samples. The basic apparatus necessary for pulsed NMR spectroscopy consists of a high-field magnet, pulse programmer, pulse transmitter, sample probe, receiver, amplifier and data recorded, along with magnetic field coils,

current generator and thermostat to control the sample's temperature.[29] The equipment needed for setup creates a disadvantage of this method as the equipment can be costly and space consuming.

Diffusion coefficient values can be obtained from chromatography, also known as Taylor dispersion. In 1953 Taylor[36] explained that for a liquid in laminar flow there is a parabolic distribution of velocities over any cross-section normal to the tube axis. Therefore, the fluid at the center of the tube moves at twice the average fluid velocity. This method is performed when a dye solution is pulse injected into a slow stream of solvent confined within a narrow tube. The color is found to move along the tube as a symmetrical column of slowly increasing length. The patch of color is not distorted as the mass transport by the bulk flow of the liquid is supplemented by diffusion. The concentration distribution within the solute column as it passes can be used to determine the interdiffusion coefficient of a two-component system. Figure 2.2 shows a schematic of a Taylor diffusion apparatus in which A is the injected dye and B is the solvent.

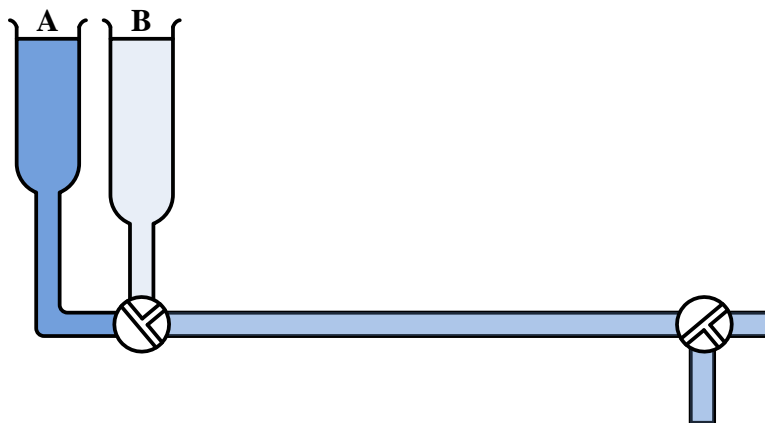


Figure 2.2 Apparatus presented by Taylor used for observing dispersion in a tube.

**Source:** [(Taylor 1954)]

While this apparatus and analysis of this method is accurate and easily obtainable, again a large solvent volume size is needed and considerably longer experimental time as compared to our micro system device we are studying.

We chose to pursue an optical measurement for a conventional testing comparison. This method is noted to be central to almost all optical methods of studying diffusion and has been documented since the 1950s and 1960s.[29]

### **2.3 Segmented flow microfluidic systems**

An interesting article by Kreutzer et al.[28] in 2008 used flow segmentation to reduce unwanted axial dispersion within a microfluidic device. By creating a second phase, separate reaction chambers of liquid, separated by gas, were used to study the diffusion flow. These pulse-broadening experiments utilized a PDMS device with fluidic cross-section channels 300  $\mu\text{m}$  wide by 300  $\mu\text{m}$  in height. A tracer is injected into carrier liquid and gas flow is controlled by a piezoelectric bending disc. Then the segmented solutions travel around a racetrack shaped microchannel that is 1.2 m or 1.77 m long. The need for the racetrack shaped microchannel is to allow large sampling as the concentration of the tracer in each segmented carrier liquid is measured by transmission spectroscopy near the outlet of the device using two polished fiber ends.[28] Figure 2.3 shows the device design and labeled components.



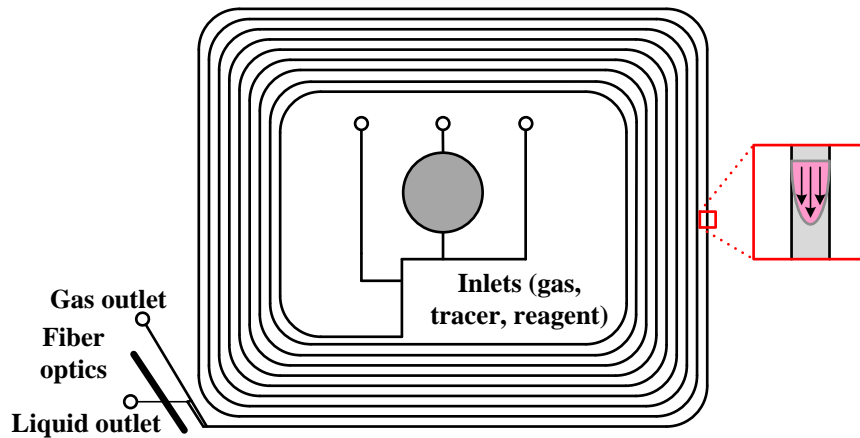


Figure 2.3 Sample dispersion study device using piezoelectric bending disc actuator and fiber optic detection. **Source:** [(Kreutzer 2008)]

One advantage over other methods this device has is with the long microchannel to the detection point; a large sample size can be obtained and compared insuring ease in statistical sampling. However, using piezoelectric bending disks and fiber optics for detection, this device is hardly a simple microfluidic device. Also, with such a long microchannel to the detection point, this device requires constant pressures and bending of the disk along with a considerable sample size.

## 2.4 Static and dynamic microfluidic systems

Culbertson et al.[3] in 2002 used a microfluidic platform to determine diffusion coefficient for electrochemical solution for a static and three dynamic methods. The three dynamic methods (stopped flow, varying applied potential and varying detection length) result in 11% larger diffusion coefficient values than static tests. Devices were fabricated using soda-lime glass and standard photolithographic techniques with depths from 10 to 15  $\mu\text{m}$  and half-depth ranging from 30 to 46  $\mu\text{m}$ . The design of the microchannels was a

simple T-structure where a buffer was introduced at the top of the T. Analyte is introduced on one side of the T and the waste is pushed by the buffer down the T out the other side. Detection was down the length of the T-microchannel. While this structure is simple in that only one layer of microchannels is needed and the volume size can be wasteful yet is within reason for the quickness of these testing methods. On the other hand, the detection method for the dynamic tests uses a common laboratory camera while the static method uses more complex detection system with a laser. All this adds the necessary equipment and complexity of this system.

## **2.5 Refractive index gradient detected microfluidic systems**

Costin[37] used a microchip based device and measured the refractive index gradient between adjacent laminar flows at different positions along a microfluidic channel to determine diffusion coefficient and molecular size using dual-beam mode of a micro-scale molecular mass sensor as the detector. The device mobile phase inlet dimensions were 500  $\mu\text{m}$  wide by 200  $\mu\text{m}$  deep with analysis channel of 3.5 cm long while the sample inlet dimensions were 100  $\mu\text{m}$  wide by 200  $\mu\text{m}$  deep and 1 cm long. While this device was accurate, it required a great deal of reagents. Polyethylene glycol at various molecular weights and sugar solutions were evaluated using this method. This system also requires the use of fiber optic splitter and fiber coupled laser diode along with positive sensitive detectors, taking the simple T-structure into a complicated analysis method.

## 2.6 Summary

Different methods for determining diffusion coefficient have been studied and evaluated for 100s of years. As we advance in technology so does the validity of conventional methods. With  $\mu$ TAS and LOC, we can reduce the sample size needed as compared to the hundreds of milliliters we once needed for diaphragm cells, and we can now use 10 nL of reagent to determine diffusion coefficient. As compared to the microfluidic systems introduced here, we want to present a multilayer softlithography device that needs no additional equipment installed within the PDMS structure and a simple laboratory camera to capture the diffusion of two reagents within a single reaction chamber of a total volume less than 25 nL.

## Chapter 3

### Development of the Diffusion Chip

#### 3.1 Introduction

The idea of measuring diffusion coefficient on a microfluidic platform is to optically observe the diffusion of two solutions into one another as related to time and calculate the appropriate observed diffusion coefficient. With our basic design of two solutions initially separated by valves, we show the basis of diaphragm cell. However, to observe diffusion like Taylor dispersion, we use pneumatic mixing valves to induce a directional flow of the two reagents into one another. This flow allows us to see a clear, initial cup-and-cone relationship between the two solutions. This is similar to Taylor's experiments in which a stream of tracer was easily seen within a steady solution. With time, the cup and cone diminish and the intensity of both solutions stabilizes to show one final observed intensity, as a constant concentration of solutions within one another. A cup and cone interfacing of the two reagents observe clear visibility of diffusion. This interfacing is where the interdiffusion takes place. From the tail of the cup and cone we can also determine the velocity of the reagent mixture within the chamber. The following schematic in Figure 3.1 represents three stages of our proposed contained diffusion. Red and green colors represent two solutions that are optically distinguishable from one another. Figure (a) shows the two solutions initially separated, similar to a diaphragm cell. Figure (b) is a step forward in time, as the two solutions start to flow about the reaction chamber in a counterclockwise manner. The beginning of diffusion between the

two reagents is illustrated with the yellowish-orange color shown between the cup and cone and tail of each reagent. Figure (c) is a further step in time, if the solutions do not diffuse well with one another, then a clear cup and cone maybe be seen circling the full reaction chamber.

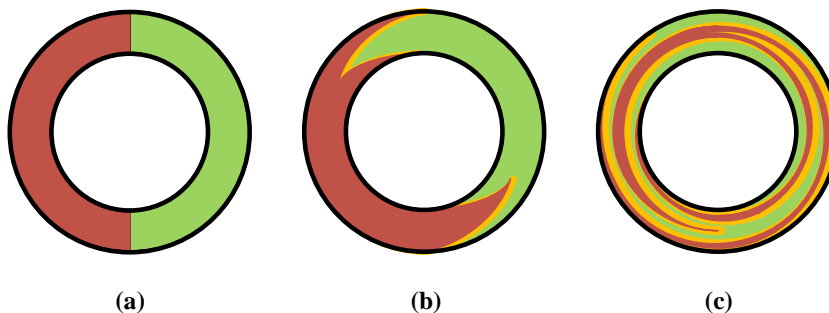


Figure 3.1 Cup and cone progression model.

### 3.2 Device design

The device is constructed out of transparent and flexible PDMS and is fabricated through a soft lithography technique. To design our device we used AutoCAD (Auto Desk) to model the structure in two dimensions. The basis of the design and three design versions will now be discussed.

All of the designs consist of two layers; a control layer in which the microvalves are constructed and a fluidic layer, top layer, in which the reaction chambers are positioned. Three separate circular fluidic systems were used consisting of two reagent in ports, two out ports, and a wash in and out system. The initial idea was to allow for all three separate reagent chambers to be examined simultaneously, given an appropriate

recording setup. However, our current experimental setup of our microscope and camera limit the clear visibility of diffusion for all three separate reaction chambers at once. Therefore, at this time we cannot simultaneously determine three separate diffusion coefficients. All three reaction chambers use the same shut off and mixing valve system, all within series of each other. The mixing valve system consist of three pneumatic valves located below the fluidic layer. Each valve is 30° separated from its neighbor valve. Previous colleges have studied at length the effects of varying valve dimensions, angle of separation, number of valves and operational frequency. From their studies we choose to use our valves for this study as follows. Various shut off control valves are located throughout the structure of the device to control the metering and direction of the fluidic reagent flow. Control channel inlets are 100  $\mu\text{m}$  in width and decrease to 30 or 50  $\mu\text{m}$ , depending on design version, near the testing system to prevent pressure interface on the circular diffusion chamber. Such interface can cause decreases in the flow of the fluidic layer and therefore is undesirable. These unwanted interfaces can be caused by large control channel widths crossing under the fluidic layer being operated at other locations and interfering with the flow of the fluidic channel it crosses under. Another way an unwanted interface can occur is by an increase of control valve pressure greater than necessary to shut the valves. The differences between the three designs are based mainly on the size of the width of the reaction chamber and the control channels.

Mixing control valves are used to induce flow of the two reagents and allow the two reagents to diffuse into one another. For clear visibility of diffusion, a cup and cone of the two reagents will show the two reagents as they diffuse into the each other in the direction of the flow. When testing various designs for this project, it was important to

clearly see the cup and cone of the two reagents. As the design versions' reaction chamber widths changed, so did the corresponding mixing and shut off control valve dimensions. Figure 3.2 shows the basis of the three designs and a close up of the reaction chamber. On the left hand side, we see the reaction chambers of the fluidic layer all colored in blue. The left side of each reaction chamber has three inlets: reagent 1, water for washing and air for drying and one outlet, and an outlet for reagent 1 for loading. On the right side of the reaction chamber, there is one inlet for reagent 2 loading and two outlets, one for washing and drying and one outlet for reagent 2 for loading. The three mixing valves are on the control layer and colored green. There are bends in mixers 2 and 3 channels before the first chamber and in between the following chambers. These bends allow for the same length of channel and thus, volume, for all three mixers to travel. This insures proper response time and even pressure for the three mixers. The remaining shut off valves are colored in red. SV1, SV2 and C are for valves responsible for metering and sectioning the solutions before each experiment. As they are a pre-test tool, the even channel lengths are not necessary. The remaining valves are all involved with the washing and drying of the chambers.

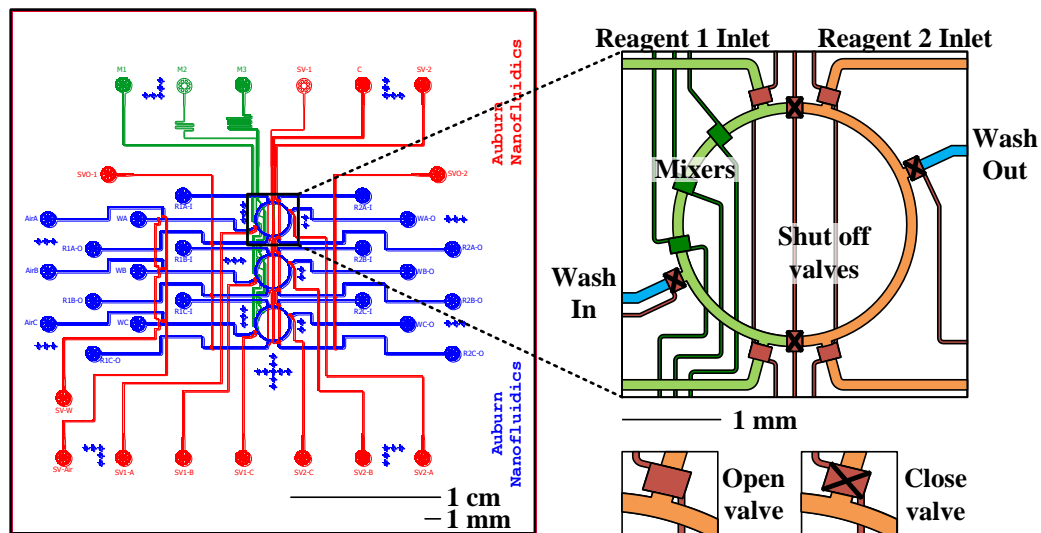


Figure 3.2 Basic design with detail of a reaction chamber and valve close/open key.

### 3.2.1 Diffusion chip design version I

The control widths start at  $100\ \mu\text{m}$  and taper down to  $50\ \mu\text{m}$ . The reaction chamber has an inner and outer radius of  $1000\ \mu\text{m}$  and  $1200\ \mu\text{m}$ , respectively. This creates a  $200\ \mu\text{m}$  testing width for a clear visual of cup and cone. Valves were created to be  $300\ \mu\text{m}$  long by  $200\ \mu\text{m}$  wide.



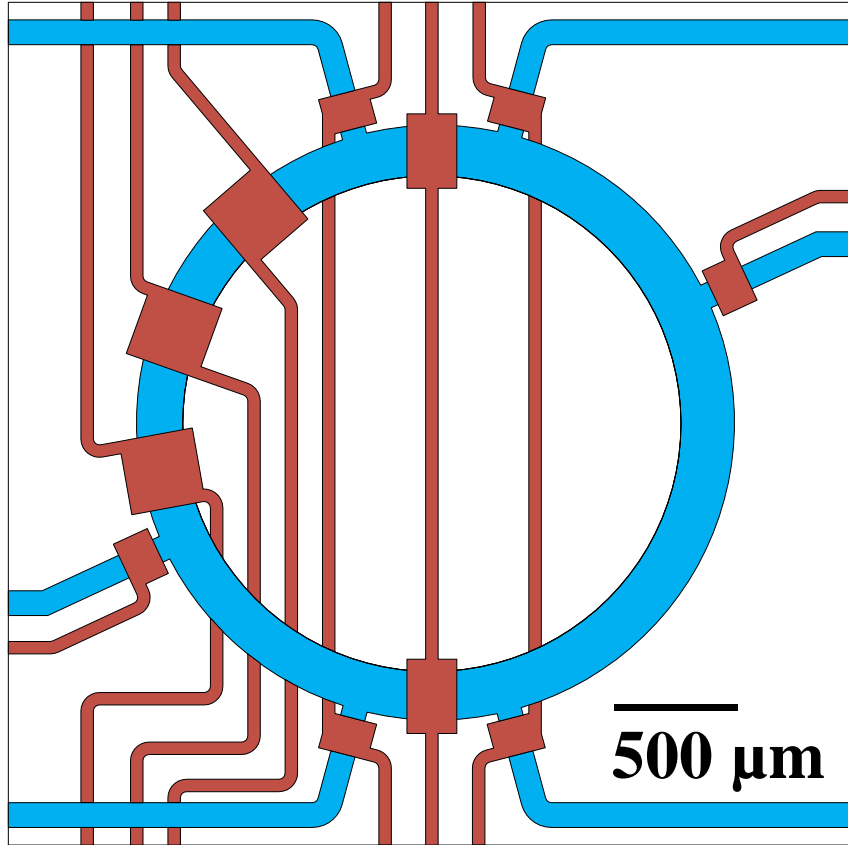


Figure 3.3 Chip design version I.

The first experiments, performed with this design, experienced problems with collapsing valves and unwanted air developing within the chamber due to great pressures needed to close the large control valves. Also, problems presented by simply trying to contain the test solutions within the reaction chamber presented pressure difficulties. All of these things are undesirable and needed vast testing parameter improvement.

Due to channel collapsing and control layer interference, we tried to level out the internal pressure of the control valves and fluidic reagent by using pressures of 15 psi and 1.02 psi, respectively. Within the 2 Hz mixing sequence, we could observe cup

and cone of the two reagents after 4 seconds, as desired. While we want to decrease the experimental test time by using the mixing valves to induce movement of the two reagents, we also need to observe the cup and cone clearly for several frames to determine the velocity. However, any collapse of a mixer valve is evident that the internal pressure within the reaction chamber is still too great for the mixing valve.

This uneven internal pressure between the two layers makes the response time of each mixing valve subject to unreliability due to possible inconsistency. Figure 3.4 is the data of an experiment using design I microfluidic device corresponding to 4 seconds from the releasing of the center valve according to the intensity/concentration reading at a ROI within the chamber valve. We analyzed the information after the center valve release, as the concentration fluctuation with time evaluation is the focus of our study to determine diffusion coefficient. However, the fluctuation presented here in this data is not ideal, compared to what we expected from the peak-to-peak relationships. We expected exponentially decreasing peaks with time as the valleys exponentially increase with time and that both time steps are similar to each other.

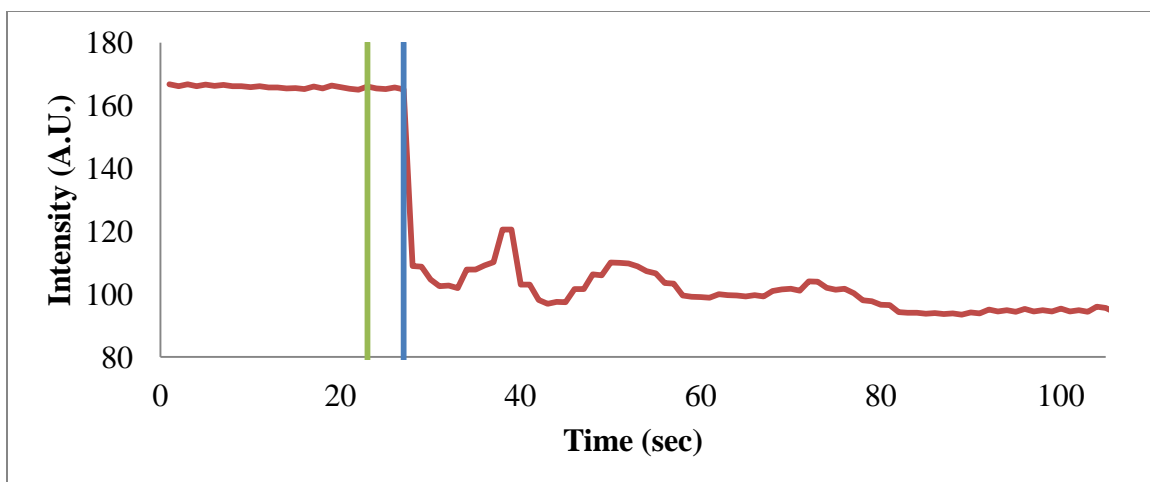


Figure 3.4 Concentration versus time data corresponding to the ROI within reaction chamber. The green line indicates the release of the center valve, thus the start of the experiment and the blue line indicates 4 seconds later.

With the problems of the reagent chamber ceiling collapsing due to the large, unsupported sections of chamber, we determined it would be appropriate to decrease the reaction chamber width and thus decrease the needed control valve dimensions.

### 3.2.2 Diffusion chip design version II

The control widths were unchanged from version I. The reaction chamber has an inner and outer radius of 1140  $\mu\text{m}$  and 1200  $\mu\text{m}$ , respectively. This creates a 60  $\mu\text{m}$  testing width for decrease valve sizes. Valves were 120  $\mu\text{m}$  by 120  $\mu\text{m}$ .

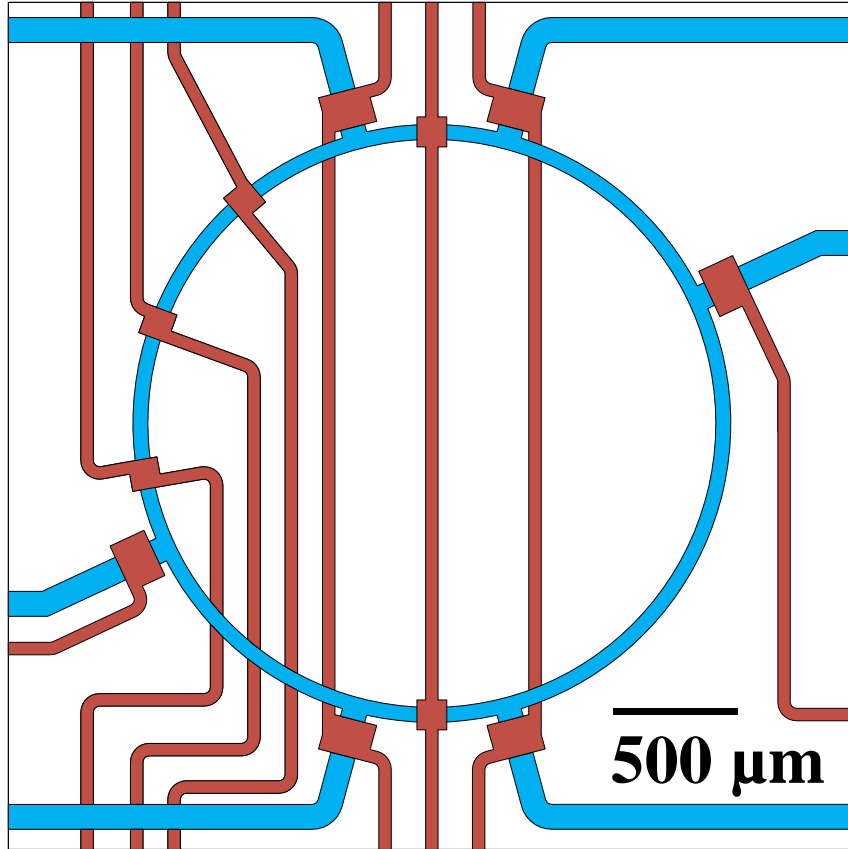


Figure 3.5 Chip design version II.

For design version II changes to the reaction chamber width and valve sizes were made to fix the problems observed in design version I with channel collapsing. However, in this design it was hard to find a suitable operating pressure combination. Figure 3.6 shows that the design change to version II does remove the problem of channel collapsing. The top mixer valve is activated in Figure 3.6; that is why it appears to have a darker channel outline than the other mixer valves. In addition, the reagent inlet and outlet shut off valves are activated in the middle left and right of the image. Since the shut off valves are filled with buffer (water) and the mixer valves are empty (nitrogen gas if activated) this explains the color and activated valve outline difference between the two

types of valves used in the micro system device. While improvements from problems were made from design version I to design version II, other problems were present with this design.

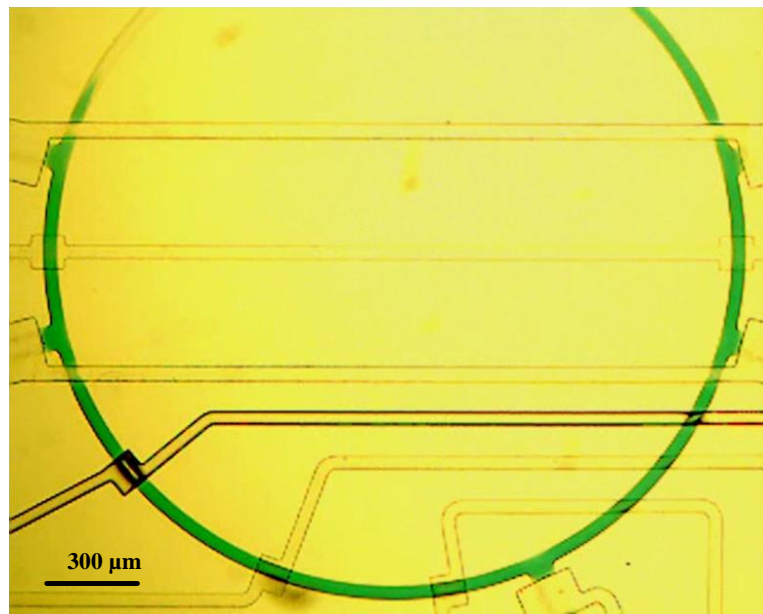


Figure 3.6 Device fabricated of design version II. No evidence of channel collapsing but shut off valves for reagent metering interferes with reagent flow.

At the points where both reagent control shut off valve channels cross the reaction chamber there is major pressure interference. To level the internal pressures prior to activating the mixer sequence the following pressures were used at 1.0 Hz, 20 psi, 15 psi, and 3.52 psi for the control valves, mixer valves and fluidic reagent loading, respectively. On the left, this causes the flow in the reaction chamber to be limited by the small amount of blue dye above the channel. This is a major disadvantage and must be prevented.

In addition, with this design version a clear cup and cone could not be seen with our given camera equipment because the experimental flow was so much faster than

design version I. Thus, preventing us from determining the velocity in that manner. As mentioned with design version II the needed pressure for closing the control valves has increased greatly from design version I. Figure 3.7 shows a center valve requiring 28 psi pressure to shut, with the reaction chamber filled with air from chip fabrication.

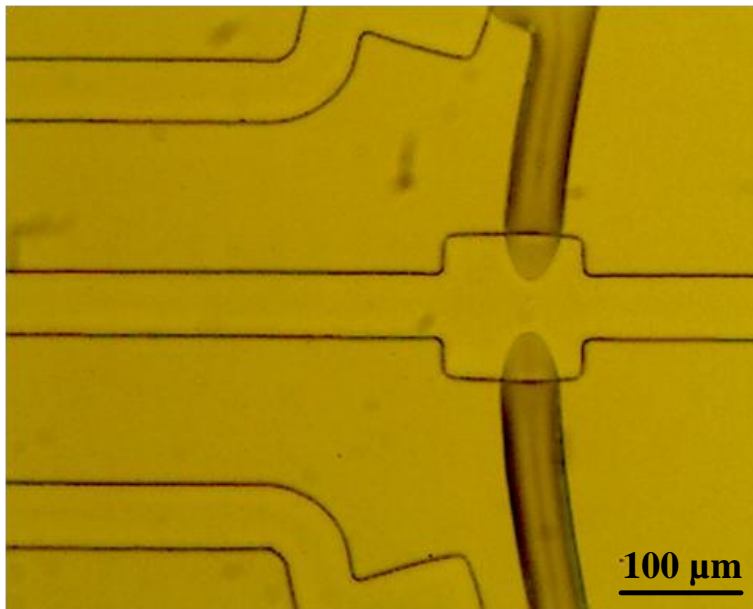


Figure 3.7 Device fabricated of design version II. Center valve with 28 psi pressure shutting valve with reaction chamber filled with air from chip fabrication.

From Figure 3.7 we can see that the valve is not fully closed. With such a large pressure for the system being applied we expect that the valve would be fully closed. With our experimental equipment system, 30 psi is the maximum pressure setting obtainable. By working at pressures of 20 psi and greater puts great, unneeded stress on the system. This makes the response, consistency, and reliability of each valve a subject of concern. With the problems of the reagent chamber interference from high pressures of control shut off valve channels and decrease in visibility of cup and cone of reagents,

we determined it would be appropriate to increase the reaction chamber width, decrease the control channel widths and increase the control valve dimensions to correspond with the reaction chamber width. We improved the micro system from the previous design; however, our disadvantages led us to redesign once again.

### 3.2.3 Diffusion chip design version III

All the control widths start at  $100\ \mu\text{m}$  and taper down to  $30\ \mu\text{m}$  to prevent pressure interface on the circular diffusion chamber. The reaction chamber has an inner and outer radius of  $1100\ \mu\text{m}$  and  $1200\ \mu\text{m}$ , respectively.

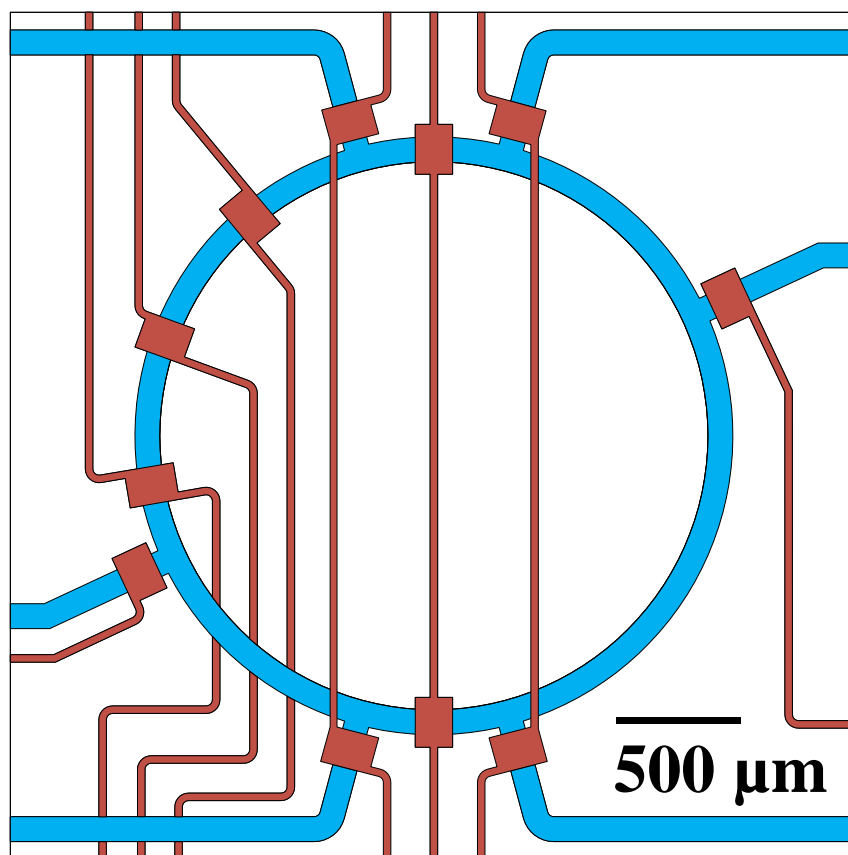


Figure 3.8 Chip design version III.

For design version III, changes to the reaction chamber width and valve sizes were made to fix the problems observed in design version II with pressure interference and cup and cone visibility. Shut off valves could be closed at appropriate pressures, such as 10 to 15 psi, and no collapsing allow for a usable, working micro system device. Cup and cone could be seen clearly and velocity could be easily determined by frame-by-frame movement analysis. Control valve channel interference with the reaction chamber was diminished due to the appropriately sized valves and decrease in control channel widths. Figure 3.11 shows a fabricated chip of design version III of a good chip. We can see the cup and cone of the two reagents and no control valve channel interference. The top mixer valve is activated in Figure 3.9 explaining the appearance difference in the valves and again the reagent inlet. Outlet shut off valves are activated in the middle left and right of the image. Like the device in Figure 3.7, the device in Figure 3.9 has buffer (water) in the shut off valves, and mixer valves are empty (nitrogen gas if activated), explaining appearance difference between the two types of valves.

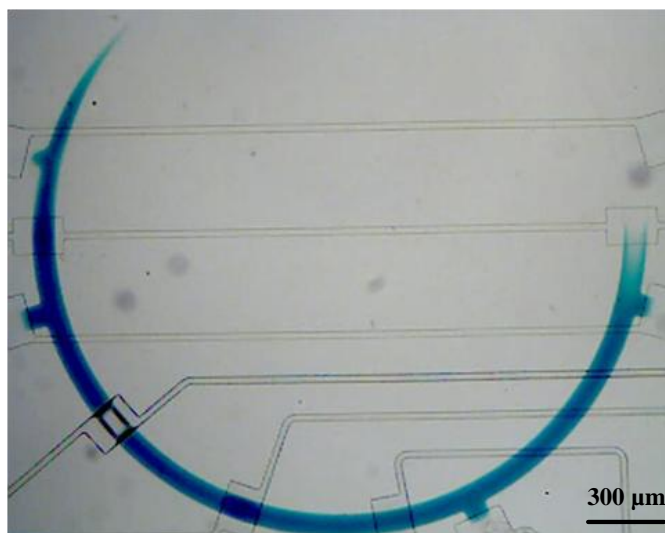


Figure 3.9 A fabricated chip of design version III of a good chip.



Also, all of the valves are working properly. The testing parameters for the device in Figure 3.9 were 5 Hz mixing sequence and the following pressures: 10 psi, 15 psi, and 5 psi for the control valves, mixing valves and fluidic reagent loading, respectively. Similarly, pressure combinations were tried for version I and version II, but did not allow for the valves to operate properly given the chamber width and valve dimensions.

Even with the great improvements made to design version III, other problems presented themselves. A problem of dye traveling inconsistently from the center valve once pressure was released was undesirable. As we want to control the fluid flow by the mixer valves this is a problem. This problem was inconsistent and therefore made our current testing parameters unreliable. Figure 3.10 shows a fabricated chip with the center valve not fully releasing its pressure after deactivation, resulting in dye solution traveling to both sides of the reaction chamber. The testing parameters for the device in Figure 3.10 was 1 Hz mixing sequence and the following pressures: 8 psi, 10 psi, and 2.04 psi for the control valves, mixing valves and fluidic reagent loading, respectively. The top mixer valve is activated in Figure 3.19, explaining the appearance difference in the valves, and again the reagent inlet and outlet shut off valves are activated in the middle left and right of the image. Like the device in Figure 3.9, the device in Figure 3.10 has buffer (water) in the shut off valves and mixer valves are empty (nitrogen gas if activated), explaining appearance difference between the two types of valves.

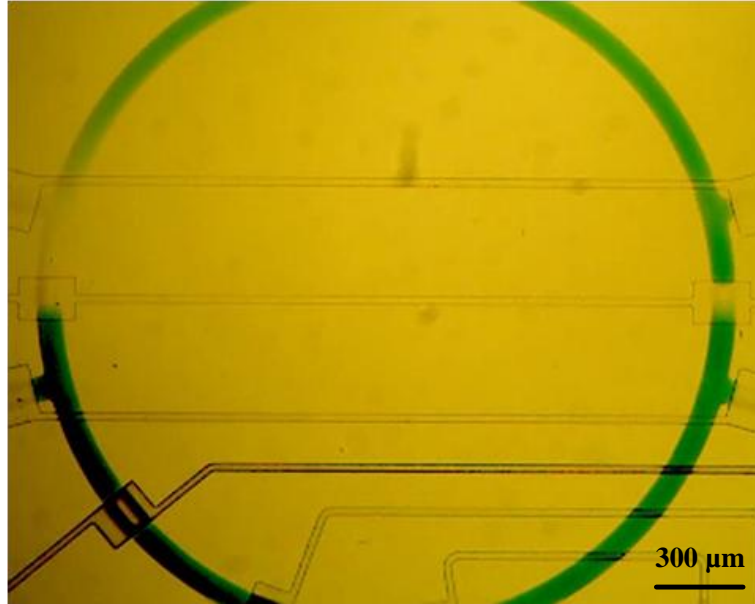


Figure 3.10 Device fabricated of design version III. Center valve pressure not disengaging properly affecting fluid flow drastically. 50.922 seconds after releasing the center valve.

Later it was determined that the control layer membrane was too thick. By increasing the spin speed of applying the PDMS to the control wafer from 2400 rpm to 2600 rpm, this problem was removed and not seen again. This shows the importance of proper selection of chip fabrication process times and speeds.

Chamber heights vary depending on master mold fabrication. Typically 10.8 μm maximum height of fluidic channel was observed. The resulting volume of reagents in a single chamber, excluding the center valve volume, is 7.53 nL. While for Design II to achieve a 5 nL volume of each reagent within the reaction chamber, a height of 11.72 μm would be needed or a height of 14.06 μm could produce 6 nL per reagent. The mold fabricated for design version II had a height of 11.32 μm, yielding less than 5 nL per reagent within the reaction chamber. Version I mold, with a height of 15 μm, would

produce volumes of 9.76 nL per reagent, while a height of 7.68  $\mu\text{m}$  would produce a reagent volume of 5 nL each. For our purposes we wanted to stay below 10 nL for convincing of the device for future endeavors. Figure 3.11 shows the device design progression from one version to another of a single reaction chamber.

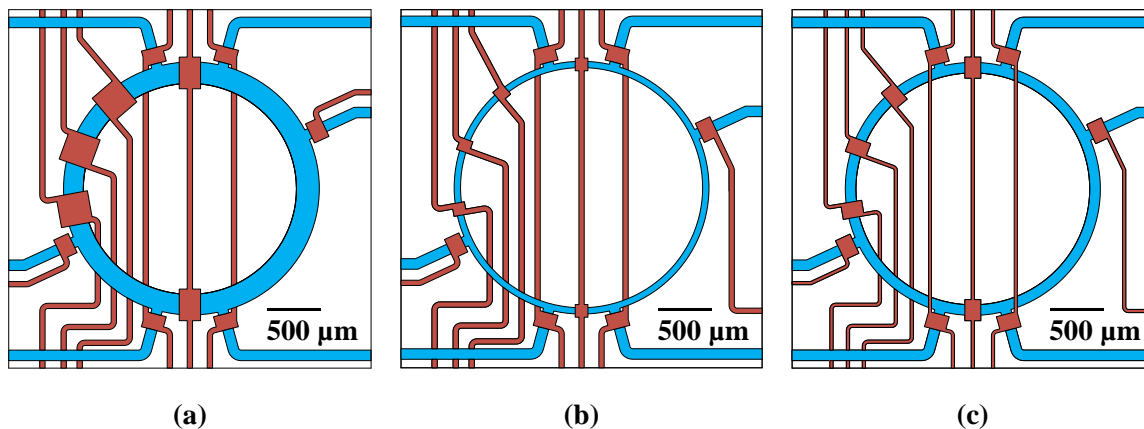


Figure 3.11 Chip design progression – reaction chamber detail view, version I (a), version II (b), and version III (c).

In a side-by-side comparison, we can see the reaction chamber width change, as well as the mixing valve dimensions. One minor change from design I to design II was the channel connection to the wash out shut off valve to the right of the chamber in (a). In design I, the control channel goes above the fluidic channel, while in the two following designs the channel goes below. This was done to reduce the number of fluidic channels that each wash out shut off valve crossed on the way to its outlet from 8 to 7. This allows the reagent to be loaded with less backpressure due to any control layer pressure interactions.

### 3.3 Mold Fabrication

Micro fluidic chips are produced by employing soft lithography method[38]. Molds are fabricated in Broun Hall in the Alabama Microelectronics Science and Technology Center (AMSTC). The center requires a safety test for permission to use the laboratory space and equipment. The center is clean room requiring proper clean room clothing and safety protection. Before entering the clean room for fabrication, the AutoCad design is sent off to CAD/Art Services, Inc. for photo printing of the design at a 20,000 dpi (dots per inch). This resolution is capable of printing a design accurate down to 10  $\mu\text{m}$ . The smallest feature size on any of the three designs is 15  $\mu\text{m}$ . Designs are printed on a transparent thin sheet of plastic and delivered sealed to prevent dust exposure.

Figure 3.12 illustrates the mold fabrication process for both a fluidic and a control layer. First start with clean 4" silicon wafers with 100 Å titanium coating. Next, spin coat photoresist onto both wafers. Then, expose that mask to the wafer using UV exposure. Develop away excess photoresist, and the pattern remains.

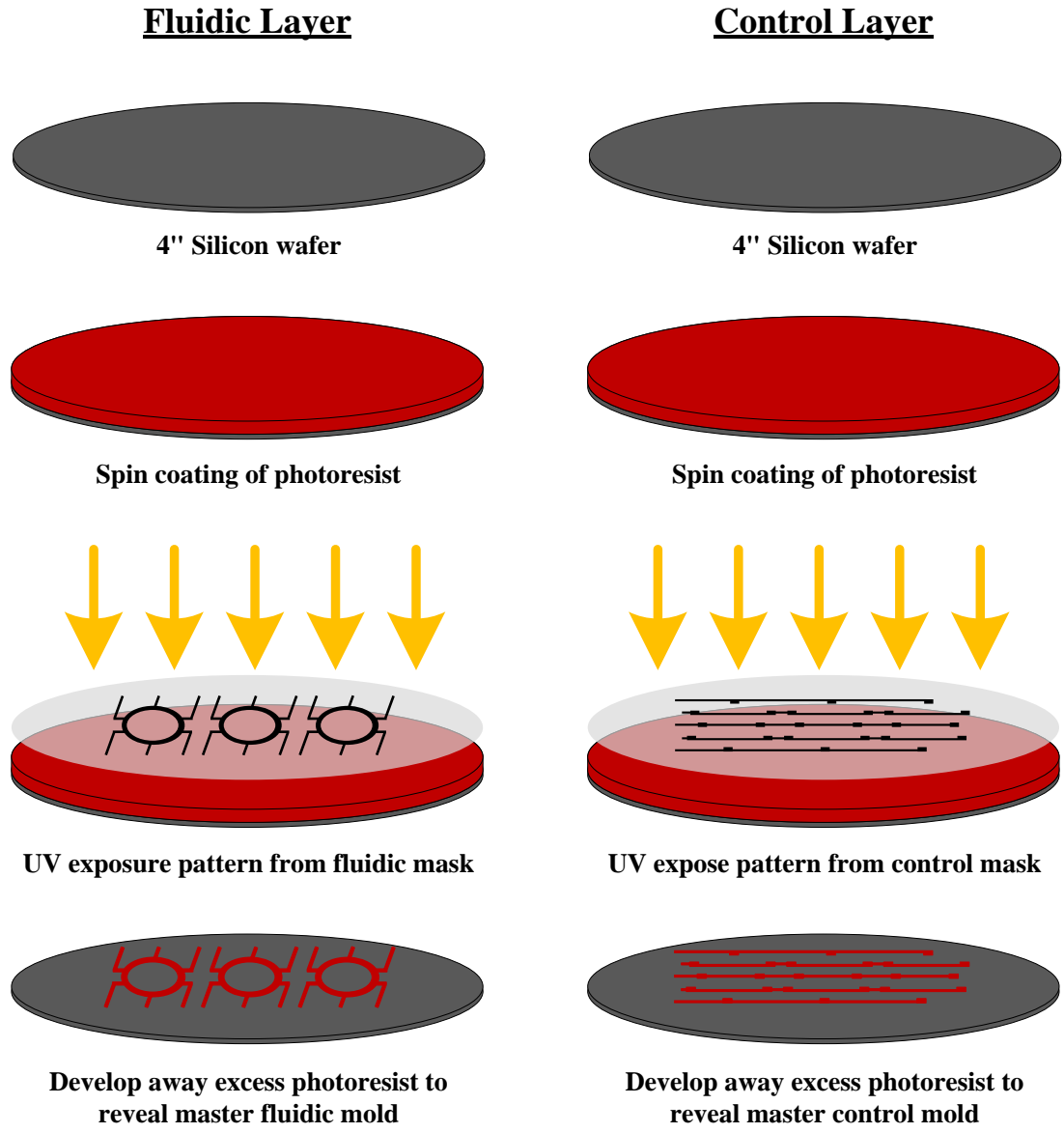


Figure 3.12 Schematic of mold fabrication process.

Full details on the mold fabrication process now follow. Before starting fabrication, once in the clean room, the mask is removed from its container and cut to shape. Then the mask is taped on four corners to a clean 4 inch by 4 inch glass plate and set aside. To begin, photoresist AZ P4620 (AZ Electronic Materials) is spun coated onto a 4 inch silicon wafer with 100 Å titanium coating followed by a 90 second soft bake at

110 °C. The titanium coating improves the adhesion of photoresist to the wafer surface and the lifetime of the mold. The spin speed settings determine the height of the structures, with slower speed resulting in higher channels. These molds were produced at a setting of 500 rpm for 5 seconds at 100 rpm/second acceleration followed by immediately by 1300 rpm for 35 seconds at 300 rpm/second acceleration. Next the mask and glass plate are mounted into the UV exposure machine (Karl Suss MA6/BA6). The structure on the mask is then exposed onto the wafer by hard UV exposure. The machine has an intensity of 19 mW/cm<sup>2</sup>. To copy the pattern onto the wafer, the transparent mask is exposed to a certain amount of UV light. The part of the mask that does not have anything printed on it will be excess photoresist and removed later. The amount of UV light or dose is controlled by the exposure time and light intensity. The dose can be calculated as follows[39]:

$$dose (mJ / cm^2) = intensity (mW / cm^2) \times time (sec) \quad (3.1)$$

As the equipment in the AMSTC clean room has an intensity of 19 mW/cm<sup>2</sup>, the time can be calculated according the dose wanted. Dose sizes should be different according to the thickness of the desired structure; a thicker structure requires a greater dose. With an intensity of 19 mW/cm<sup>2</sup> and a desired dose of 600 mJ/cm<sup>2</sup>, a 31 second exposure time at hard contact is appropriate.

The exposed photoresist is developed away by placing the wafer in a plastic bin and agitating it back and forth within 200 mL of AZ 400 K 1:4 diluted developer (AZ Electronic Materials) for 2-4 minutes. Since AZ P4620 is red, as the photoresist is being

developed, the liquid will turn pink. After developing, the wafer is then rinsed 3-5 times with deionized water and air-pressure dried. Next, the wafer is inspected under the microscope to insure the photoresist has been fully removed. The final step in the control mold making is checking the height of the structure. Using a refileameter (Tencor) measure the structure at numerous locations to insure that the structure is the same height all around. Once this is done, the control layer is complete. After measuring the fluidic layer, a final post-bake at 130 °C is preformed for 3 minutes to round the channels. The height is measured again with the refileameter and the mold is complete.

Control mold height was observed to be on average 10.60  $\mu\text{m}$  and after a post baking, the fluidic mold channels were 10.8  $\mu\text{m}$  on average.

### **3.4 Chip Fabrication**

Since the control layer's ceiling will need to be raised as air pressure is applied to the channel in the control layer, the control layer needs to be more elastic than the fluidic layer. Thus the fluidic layer should have a 1:10 PDMS ratio and the control layer shall have a 1:20 PDMS mixing ratio. This allows for less cross-linking in the control layer making it more elastic.

Table 3.1 and Figure 3.12 illustrate the chip fabrication process starting with the two separate layers, then with the completed chip. First, a mold is fabricated as discussed in section 3.3 of this thesis. Next, PDMS is poured and spun to the appropriate wafers. Then, the PDMS is cured, exposing the microchannels within the PDMS. The inlet holes for the fluidic layer are punched and the fluidic layer is aligned onto the control layer. After proper curing, the two layers are removed from the control mold and the control

layer inlets are punched. Lastly, the two layers are placed onto a glass substrate covered with cured PDMS and the chip is complete minus a final, long curing step.

Table 3.1 Soft lithography chip making procedures.

Fluidic Layer Mold	Control Layer Mold
Prepare RTV 615 mixture A : B = 10 : 1	Prepare RTV 615 mixture A : B = 20 : 1
Vacuumize RTV 615 Mixtures (2 hour)	
Covering (A:B=15g:1.5g, 1.5 hour) and Surface Treatment with CTMS* Vapor (10 min)	
Make Aluminum Foil Mold	Spin Coating (2600 rpm, 1 min)
Pour RTV 615 Mixture onto Mold	Leveling (15~30 min)
Keep in Oven at 80°C (60 min)	Keep in Oven at 80°C (45 min)
Natural Cooling (10~15 min)	Natural Cooling (10~15 min)
Cut, Peel, Reverse and Punch Holes	
Fluidic Layer is Aligned with Control Layer	
Keep in Oven at 80°C (1 hour)	
Cut, Peel, Reverse and Punch Holes	
Seal Chip with Glass Slide and Keep in Oven at 80°C (18 hour)	

\* CTMS, Chlorotrymethylsilate



**Fluidic Layer**



**Master fluidic mold**

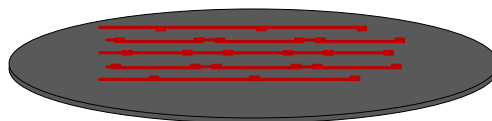


**PDMS thick layer framed onto mold**

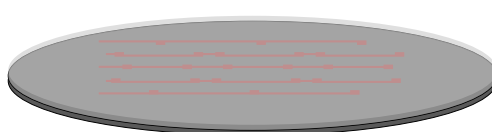


**Fluidic pattern cured into PDMS**

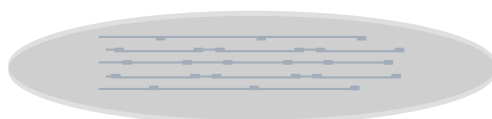
**Control Layer**



**Master control mold**



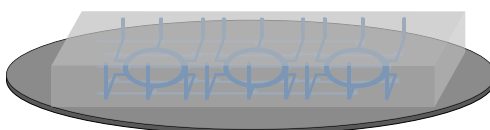
**PDMS thin layer spun onto control mold**



**Control pattern cured into the PDMS**



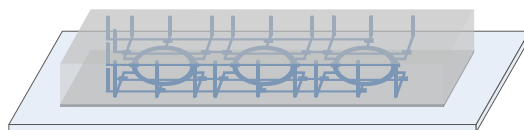
**Punch inlet holes for fluidic layer**



**Aligning two layers together**



**Punch inlet holes for control layer**



**Complete chip on glass slide**

Figure 3.12 Schematic of chip fabrication process.

The first step in making a microfluidic chip is preparing 2 mixtures of PDMS that will be used for the different layers. For the control layer, a 1 to 20 ratio (1 part RTV615 B-cross linking agent and 20 parts RTV615 A- silicone potting compound) of PDMS is needed. It is best to measure out component B first since in both mixtures will have a smaller amount of component B than A. Depending on the desired thickness of the control layer and adhering layer of the glass substrate (used later) a full 20 grams of A and 1 gram of B might not be needed. Usually 16 grams of component A and 0.8 gram of component B will work.

For the fluidic layer, the top layer where the fluid is introduced into the chip, a desired thickness is 5 mm. Usually a 45 gram A and 4.5 gram B will be sufficient; the amount depends on how large the frame of aluminum is created around the system.

Measure out the B component into a small 3” plastic weighing dish and then zero the scale and add the A component right on top of the B component. Use a disposable plastic pipette to mix the solution for 5 full minutes. To remove any remaining PDMS from previous fabrication, pour a small amount, about 8 grams, of the 1:10 mixture onto each wafer, cover and place in the oven set at 80°C to cure. Place the remaining PDMS mixtures in vacuum to remove bubbles you introduced. Cure the PDMS on the wafers for at least 45 minutes. However, we generally will cure for 60 min and vacuum for 90 min or 90 min and 120 min, respectively. This cleaning layer of PDMS on each wafer prepares the wafer for use by removing any remaining PDMS or particles from previous fabrication use. Wafers, if keep properly, may be used for years. This insures consistency in device structure for fabrication. Cleaning layers maybe applied and cured after fabrication to decrease the next fabrication prep time needed.

After cure time is up, remove wafers and let cool for a few minutes (2-3). Remove PDMS carefully and place wafers in clean petri dishes. Chlorotrimethylsilane (CTMS) treatment is optional. However, it improves the lifetime of the photoresist on your wafers and prepares the surface for the PDMS.

Under a fume hood we use a large flat beaker (see images) with a small 40 ml beaker sitting inside. Tear approximately a 12 x 12 inch square of aluminum foil and fold it over the large beaker securely. Remove foil and place aside for the moment. With CTMS, carefully remove cap and pour about 2-5 mL into the small beaker. Make sure this is all done under the fume hood as the liquid is extremely flammable and vapors are dangerous and can cause cancer. Put the small beaker in the middle of the large beaker. Next using the wafer tweezers, transport the wafer from its Petri dish to the large beaker. Next, position the wafers so that one part is resting on the small beaker (see picture). Re-cover the large beaker using the aluminum foil shaped earlier. Let wafers stay in CTMS treatment for 10 minutes. Once time is up, remove aluminum foil and wafers, and let remaining CTMS evaporate under the hood.

Once vacuum is done, turn the vacuum off. Turn on the spinner, coat the inside of the spinner with aluminum foil for easy clean up and turn on vacuum and nitrogen for spinner. Remove the 1:20 mixture; remove any bubbles and particles (usually around the edges) with a disposable plastic pipette. Place control wafer in center of spinner, apply vacuum, and do a test spin run to insure it is properly centered. Using the nitrogen gas valve, spray off any possible dust from the wafer. Currently I am using a program with 2 steps: step 1, 60 seconds, 2600 rpm, 256 rpm/s acceleration; step 2, 20 seconds, 200 rpm, 256 rpm/s acceleration. The first step dictates the thickness of the PDMS layer, while the

second step is primarily used to slow down the wafer. Start pouring the 1:20 PDMS mixture into the spinner bowl and then onto the wafer itself. Start pouring PDMS away from the chip so that you leave less possibility for bubbles to form. Pour most of the mixture onto wafer and then go back to the spinner bowl, just like the way you started. Next using a disposable plastic pipette, remove any bubbles and possible dust from the wafer. Once that is complete, close the lid and press 'Run Stop' button. Once spinning is complete, open lid, press 'Vacuum' and place wafer back into its Petri dish. Place wafer on flat surface (we have levels to show the appropriate places) and allow wafer to level for 15 to 30 minutes. Coating the glass slide with PDMS is optional and steps are as follows: Once you place wafer in leveling area, clean a glass slide using the 70% ethanol push bottle (30% water) and the lab wipes. Then place the glass slide in the spinner and repeat the same steps for the glass slide. However, the glass slide can level until the wafer is done. Turn off the spinner and vacuum when done.

While the glass slide and wafer are leveling, prepare the fluidic layer for PDMS. Using aluminum foil, tear off about a 10" x 10" sheet, then place the fluidic wafer in the middle. Fold the edges of the aluminum foil up to the wafer design leaving at least a half a centimeter between the aluminum walls and the outer edge of the design. The aluminum foil walls should be at least one centimeter high. Using nitrogen, spray off any possible dust from the aluminum foil and wafer structure and turn off nitrogen when done. Press down carefully and make sure aluminum is secure to the wafer. Remove the 1:10 PDMS mixture from the vacuum and remove bubbles and dust using a disposable plastic pipette. Slowly pour the PDMS into the aluminum frame. Again, remove any possible dust and bubbles afterwards. Place petri lid back on when done. Now put both

wafers and glass slide into the oven at 80°C once the leveling time for control layer has completed.

After 45 minutes remove the control layer wafer and glass slide and after 1 hour from original introduction, remove the fluidic layer wafer. Let the fluidic wafer cool for at least 5 minutes before continuing.

After letting the fluidic layer cool, put back on gloves and get out a ruler and the Exacto knife. Clean off the ruler and Exacto knife blade with ethanol solution push bottle and the lab wipes. Next, try to bend back parts of the aluminum structure that did not come in contact with PDMS to make the aluminum frame level with the PDMS. You next want to cut the PDMS structure out into the shape of a rectangle outside of the rectangular parameter photoresist pattern. Place a ruler across the PDMS and cut with the Exacto knife at least 0.5 cm away from the outline of the structure. Try to make smooth cuts and do not try to cut all the way down to the wafer in the first cut, make several passes progressing in depth each time. Do this for all four sides. Once all sides are cut, carefully pull back the excess PDMS and remove the aluminum foil. Then slowly peel off the fluidic PDMS layer from the wafer. Place PDMS structure with the pattern up onto a cleaned glass slide. Throw away the excess aluminum foil and PDMS.

Next punch inlet holes using a microscope. The microscope we utilize is a Nikon SMZ 800 microscope (Model C-DS). Press the hole punch in a indicated hole area. Then carefully, with the hole punch still in, remove the fluidic layer from the glass slide and place a finger behind the hole punch and press through. Remove the excess PDMS and slowly remove the hole punch. Place PDMS structure back on glass slide, clean the hole puncher and repeat until done. Once all holes are punched, clean the surface of the

PDMS with tape. Cover the surface with a layer of tape and remove. Do this until it is free of dust and particles.

Next, align the control layer with the fluidic layer, the pattern side of the fluidic layer should go downward. Use the cross-hairs as aligning indicators; all plus signs on the control layer should align with the fluidic plus signs. Take your time and get it right. It takes practice to get this right and time needed can be reduced with practice. Once aligning is complete, clean the surface of the control layer with tape like before. Once done place petri dish lid back on and place in oven for 60 min, depending on chip design.

After the required curing time has passed, remove chip and let cool for 10 minutes. Use scapula knife, cleaned with ethanol solution, to cut along the edges of the chip. Once that is done, slowly lift chip starting at one side to remove from wafer. Next, place on clean glass slide and punch any remaining holes like before. Once all holes are punched, place chip with pattern down on the spun glass slide from earlier. It is important to inspect the device for any collapsing channels prior to the final curing step. Collapses noticed was during chip fabrication usually are due to the large surface area of the inlets. All of these collapses can be fixed easily by introducing small amounts of air into the device through the fluidic inlets to equalize the internal pressure between the two layers. Air is introduced through the inlet of the channels using a syringe, Tygon tubing and tubing-to-device needle. Make sure there is no air bubbles between the two layers. Place chip back into oven at 80° for at least 18 hours.

### 3.5 Experimental setup and operation

The chip is operated using gas pressure to control the valves, and fluid movement is induced by pressure delivered from nitrogen gas. Pressure for each channel is delivered from the nitrogen tank to a pressure controller (Fluidigm) to a solenoid valve (The Lee Co., 12 VDC, 40 psig) to the chip, through a series of Tygon tubing. Figure 3.13 shows a completed microfluidic chip made from design III, filled with food dye for visualization. It is connected to Tygon tubing and includes a quarter for size comparison. Like Figure 3.2, the control layer is indicated with red, mixer channels with green and fluidic channels with blue food dye.

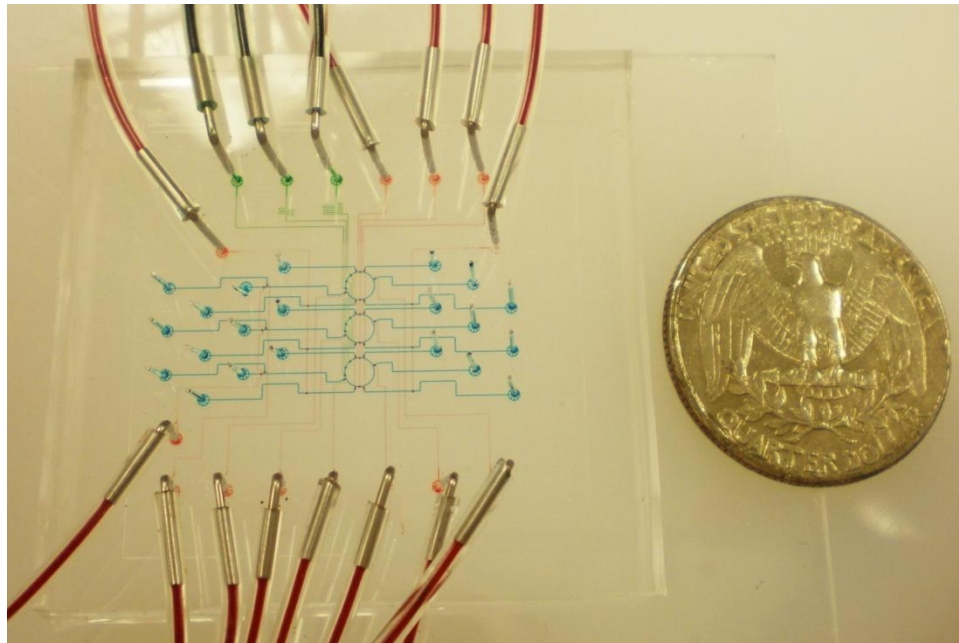


Figure 3.13 Microfluidic chip made of design III filled with food dye for visualization of structure, connected to Tygon tubing and includes a quarter for size comparison.

Control valve tubes are filled with de-ionized water as a buffer solution and is pumped into the channel at a low pressure, approximately 2-3 psi. This is not done to the mixer valves; to prevent lag time of induced gas pressure to activate and deactivate the mixing valves, these tubes remain free of buffer (water) solution. All miniports are connected to a BOB3 operating system, which is then connected to a computer operated by LabVIEW software. Figure 3.14 shows a schematic of our experimental equipment setup.

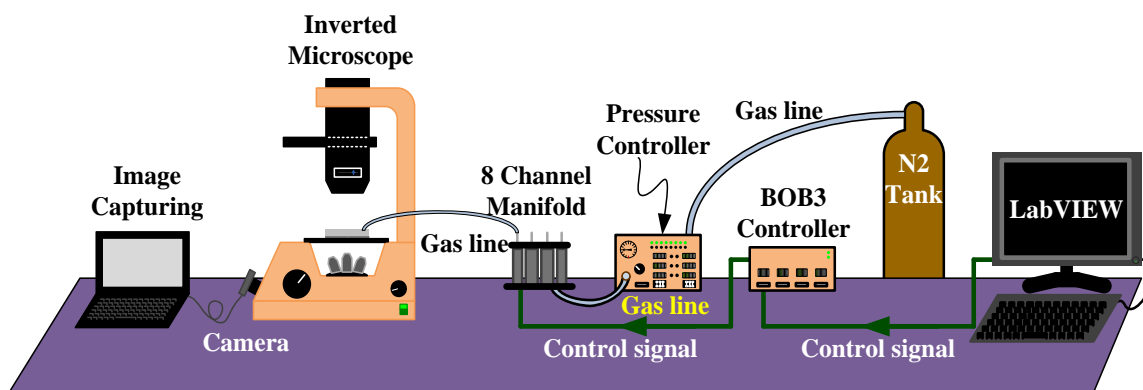


Figure 3.14 Schematic of experimental setup.

We use LabVIEW to create a single step, repetitive mixing sequence to observe the oscillation of inter diffusion of the two reagents. The mixing valve sequence as discussed in section 1.4.2 is as follows: (100, 010, 001). Constant fluidic pressure is set to approximately 5.0 psi ( $\pm 0.05$  psi) and the control valves and mixers pressure is set to 10 and 15 psi, respectively.

Details of the operating procedures for a single test include the following steps. For operation of the device, first the center valve and side wash valves, one on each side, are closed separating the reaction chamber into two separate but equal parts. Next,



reagents are loaded into the dry chamber parts. It takes a matter of a few seconds to introduce the reagents to the chambers. To insure even pressure throughout each half, reagents are allowed to flow an additional 3 minutes. For industrial uses, this additional loading time may not be necessary. Once loaded, the shut off valves to the reagent in and outs are activated and pressure-pushing reagents are deactivated. Figure 3.15 illustrates the step-by-step operating procedures for a single reaction chamber experiment.

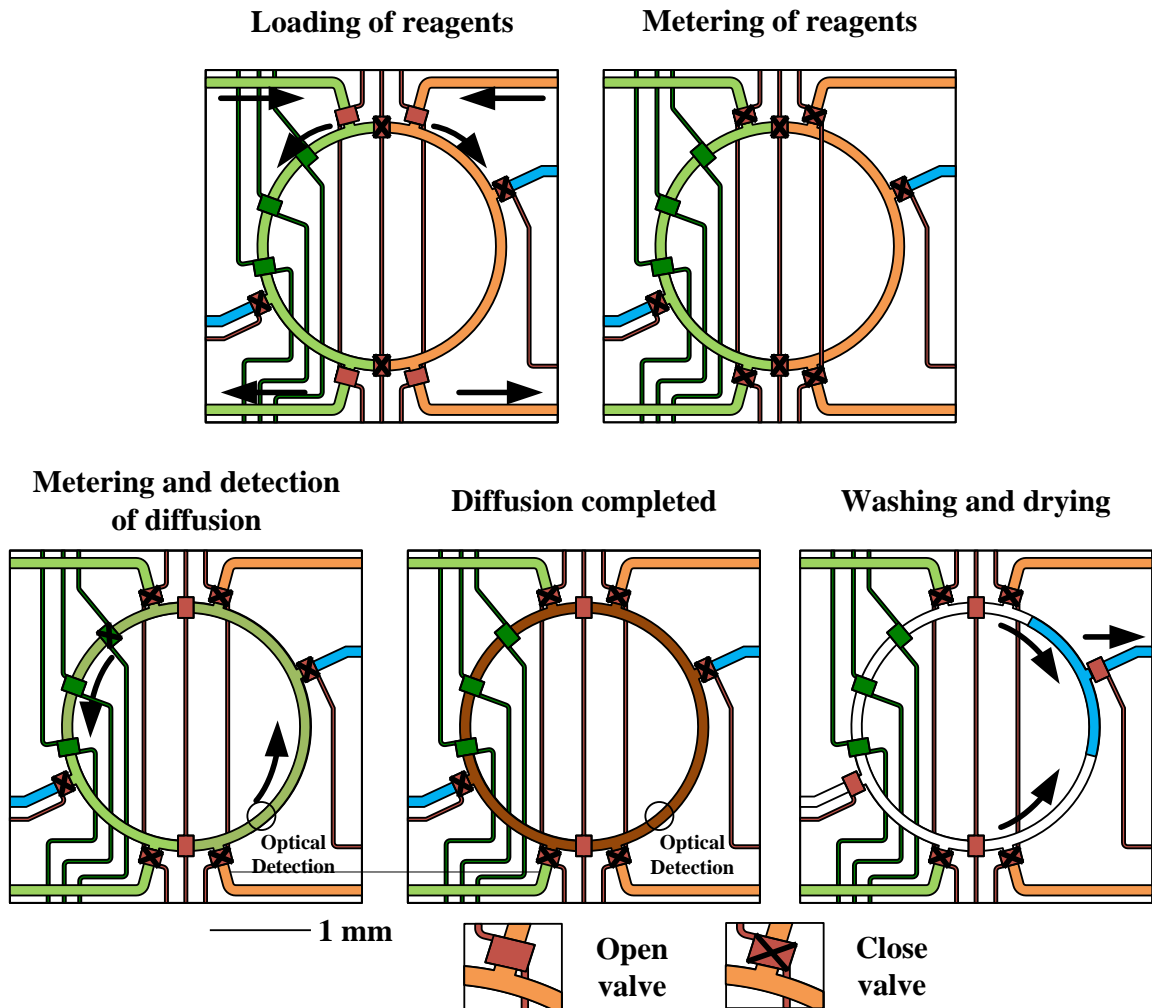


Figure 3.15 Schematic of experimental operational procedures.

Next, the camera is activated to record the following experiment. Within our lab, we use a Motic 1000 1.3M camera connected to the inverted scope of our Zeiss Axiovert 40 C/CFL microscope. Next the mixing valve sequence is started, quickly followed by the release of pressure to the center valve. This allows diffusion of the two solutions to begin. Once testing is complete, the mixing sequence is stopped and the wash in and out valves are opened. First, the chamber is washed with de-ionized water for a approximately two minutes at constant pressure, followed by drying with nitrogen gas at constant pressure. Once dry, the operation can be performed again. All reagent, water and drying are at the same constant pressure to allow for constant testing parameters. The blue and yellow filled areas represent reagents and were used to aid in visualization of the devices' functions and do not indicate the color of the reagents used.

A video is recorded at 2.5 X or 10 X magnifications using a Motic 1000 1.3M pixel camera and Motic Images Plus 2.0 program. Video is started before releasing the center valve and stopped after approximately 3 to 5 minutes of mixing valve sequence operation. The camera is mounted to a Zeiss optical microscope (Axiovert 40 CFL, Germany). The videos are first separated into image sequence of each test using Virtual Dub, then uploaded into Image J software. Utilizing Time Series Analyzer V2.0, a plug in for Image J software, a ROI, region of interest, is selected within the testing chamber on the reagent two side of the testing chamber and an average intensity is calculated for each image.

### **3.6 Results and discussion**

The diffusion coefficient is represented in terms of centimeters squared per second. Visual light intensity is comparable to concentration because in this method we are looking for the change in concentration per time. Before allowing diffusion to occur, the water side has a high and steady state visual intensity. Once diffusion is allowed to occur, shut off valves are opened, and the blue food dye diffuses into the water decreasing the visual intensity value. The visual intensity value oscillates from low to high as the two reagents diffuse into one another and advance around the testing chamber until a steady state visual intensity value is observed; this is lower than the starting water intensity. The intensity change can be correlated to the concentration change of dye in water.

The software Image J allows the average intensity of one area to be calculated given a set region of interest (ROI). We used an oval ROI with height and width of 22 pixel circle in 640 x 512 pixel sized image sequence, when in 2.5 magnification using the Zeiss optical microscope.

All tests on chip were performed at room temperature at 25.0 ( $\pm 0.2$  °C) using an indium tin oxide heater (Cell MicroControls, USA). The experimental setup was similar to Taylor dispersion in that they introduced a tracer pulse in a fluid flowing in laminar flow within a circular cross section.

#### **3.6.1 Introduction**

Our plan is to validate a micro system device using optical detection of intensity fluctuation as pneumatic valves operate in sequence to create a peristaltic pump within a

closed loop. Since the observed intensity is related to the concentration, we will use the two interchangeably. Using an equation, we developed for Fourier concentration profile we plan to match the equation to the experimental concentration versus time profile through data analysis and computer programming and then calculate  $k$ , apparent or virtual diffusion coefficient from the experimental. Lastly, we will use an equation relating  $k$  to  $D$ , diffusion coefficient and determine the experimental diffusion coefficient of our reagents.

### 3.6.2 Equation validation

Jean Baptiste Joseph Fourier was a mathematician and physicist known for studying applications and problems of heat transfer and vibrations. Fourier developed many analytical relationships for heat transfer. In Crank's second addition of The Mathematics of Diffusion[2] he explains in detail how conversion of heat flow to diffusion solutions can be done given Fick's second equation and the corresponding equation for heat flow. This allows  $\theta$ , temperature to be analogous to  $C$  for concentration and  $K$ , heat conductivity, with  $D$  for diffusion coefficient. This allows us to use Fourier's relationship for varied movement of heat in a ring to determine the apparent diffusion coefficient. We modified the original Fourier's concentration profile equation from Fourier's 1878 Analytical Theory of Heat to suit our analysis [31].

$$C(x,t) = C_m + \sum_{n=1}^{\infty} \exp\left(-\frac{4n^2\pi^2}{L^2}kt\right) \quad (3.2)$$

$C(x,t)$  represents the concentration as related to distance and time,  $C_m$  is the final average concentration.  $U$  is the velocity of the solution, cm/s, while  $L$  is the length of the system, or in our case the circumference.  $t$  is time, in seconds, and  $k$  is the apparent diffusion coefficient, cm<sup>2</sup>/s. The apparent diffusion coefficient has been related to the diffusion coefficient relationship by Taylor 1953 [36].

$$k = \frac{R^2 U^2}{48D} \quad (3.3)$$

$k$  is the apparent diffusion coefficient and  $D$  is the diffusion coefficient, both in units of cm<sup>2</sup>/s whereas  $R$  is the radius of the diffusion tube, as related to Taylor dispersion, cm, and  $U$  is velocity, cm/s. From these two equations we can expect our concentration versus time profile to look similar to Figure 3.16.

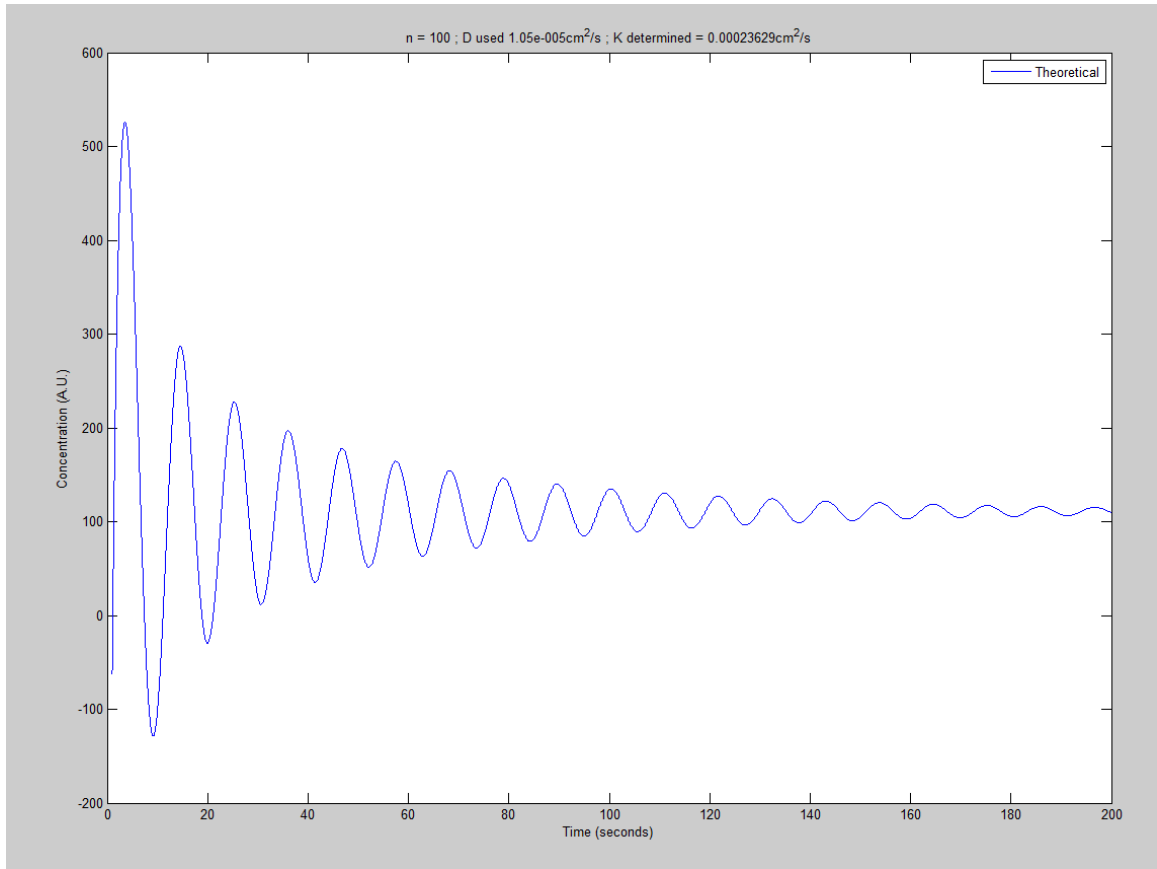


Figure 3.16 MATLAB plot of theoretical concentration versus time profile given the Fourier concentration profile and experimental and known values.

Figure 3.16 was developed by entering the diffusion coefficient value from Pratt et al.[40] at  $1.05 \times 10^{-5} \text{ m}^2/\text{s}$ , using our circumference of 0.7226 cm as  $L$ , half of our testing chamber width at 0.005 cm as  $R$ .  $U$  and  $C_m$  we observed experimentally as 0.0674679 cm/s and 111.037 (A.U.), respectively.  $n$  was set at 100.

The equation validation plan is to fit the experimental data with the theoretical equation, to an appropriate degree of error, and calculate the corresponding  $k$  and  $D$  values. Then, compare the experimental determined  $k$  and  $D$  values with known values and evaluate. Proper testing parameters such as operating pressures, mixing frequency

and sequence should allow for reproducible and reliable experimental microfluidic results. However, the testing parameters are not known for this particular experimental determination and therefore will require evaluation and determination of ideal testing parameters.

To determine the proper testing parameters, we have some expectations from prior experience. These expectations will now be discussed. For control to fluidic pressure ratio a working ratio of 2:1 should be observed. To accommodate this ratio, the internal pressure within the fluidic channels must be limited such that the thin membrane of PDMS from the control channel does not become collapsed to the substrate by the weight or pressure exerted by the fluidic channel. Thus, no collapsing should occur before, during or after an experiment. A clear cup and cone of the two reagents should be distinguishable at the beginning of each experiment, so that the velocity may be determined. Proper selection of a mixing frequency is also needed as related to the mixing valve sequence of operation. Given the same mixing valve sequence, an increase in frequency should result in a decrease in time to a constant concentration and vice versa. Also, with an increase in frequency we would expect shorter time difference between peaks and valleys compared to a lower frequency. This increase may also induce unsteady, erratic shifts in concentration as compared to lower frequency allowing the concentration to steadily increase and decrease as the two reagents diffuse into one another. Following these considerations, we evaluated each design version and corresponding data validity. Through which, the third design proved improved reproducible devices with favorable response times. Extensive testing for determining the proper operating parameters were evaluated. From the testing operating procedure

experiment comparisons, we determined water and dye had smoother curves and therefore would be ideal for initial validation of the theoretical equation as compared to ethanol and dye experiments. Other procedures chosen were standard mixing sequence of (100, 010, 001), as it produced smoother curves for water and dye than compact mixing sequence, and 5 Hz mixing sequence, as it produced faster results. In addition, mixer sequence activated before the center valve released was chosen as our results were inconclusive, and that was our common practice before these experiments. Therefore we performed more experiments using the above testing operating procedures and reagent combination to give the following concentration versus time profile as seen in Figure 3.17.

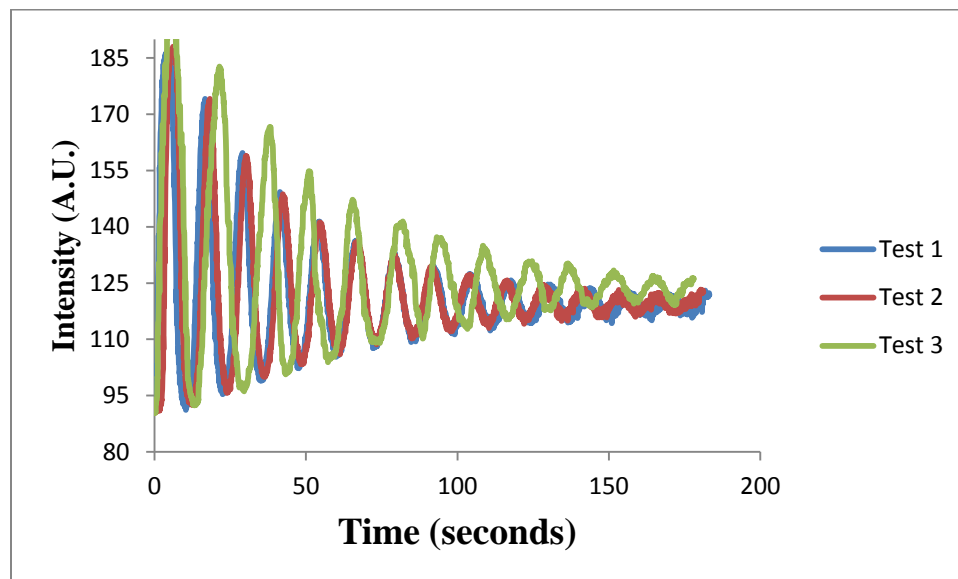


Figure 3.17 Concentration versus time profile of two experiments at 5Hz, standard mixing sequence of water and dye.



To validate the diffusion equation we chose the experimental conditions, as it appeared similar to our theoretical curve. The three experiments were performed using the same testing parameters and the same microfluidic chip, one after the other.

### 3.6.3 Data analysis

From the observed intensity fluctuation trend, a relationship with the following equation can be used to determine the observed diffusion coefficient. The peaks and valleys of the experimental data are evaluated to determine the diffusion coefficient. For the baseline dye and water experiments, Figure 3.18 shows the averaged peak and valley points with regards to time from the three tests.

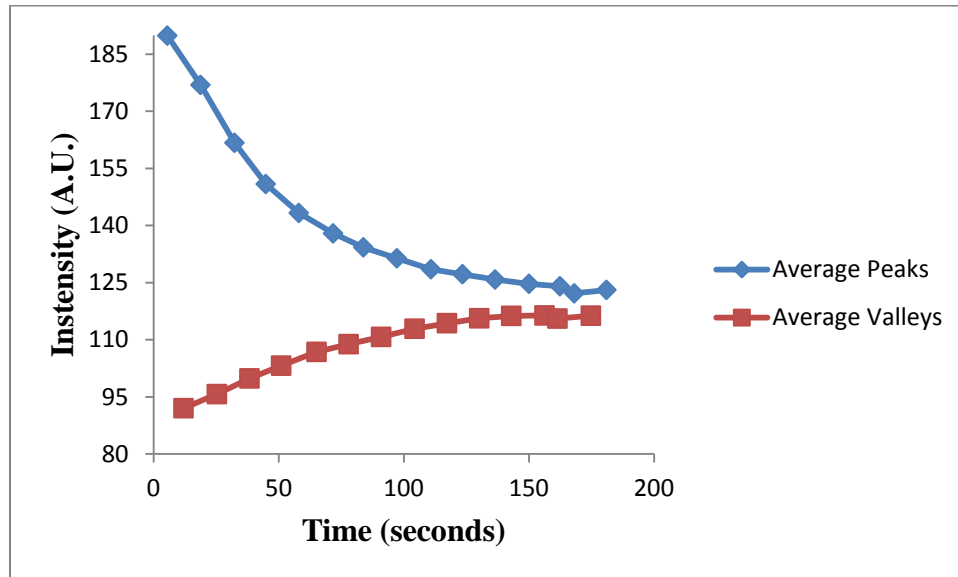


Figure 3.18 Average peak and valley points from test 1, 2 and 3 from Figure 3.17.

All data was normalized by comparison with a standard light intensity reading during each test off set from the experimental diffusion area. The first valley peak was

chosen at the start of the experiment. While there was no mixing occurring prior to this point, there was some slight variance in light intensity due to experimental setup. To better reflect the true first valley point the presented point was chosen as compared to the smallest intensity recorded. Figure 3.18 data of averaged peak and valley values are used in the remaining analysis procedures.

#### 3.6.4 SPSS analysis

Since we have one equation and 1 unknown ( $k$ ) we choose to curve-fit of the exponential of the peaks and valleys to the exponential part of the theoretical equation. We assume that the exponential curves of the top and bottom of the theoretical equation will give us an appropriate approximation of  $k$  and therefore  $D$ . MATLAB curve fit functions were not appropriate giving poor R and R square values and curves with less than adequate fit. The resulting equations were linear looking and curved slightly, in the opposite direction. Consequently, we used SPSS program (Statistical Package for the Social Sciences). SPSS is a computer program used for statistical analysis, among other things (IBM company). From the regression analysis options we choose three options that seemed the most promising for accurate analysis. Logarithmic, cubic and power regression equation analysis were chosen. Their corresponding equations are as follow.

Logarithmic SPSS regression analysis expression

$$Y = b_0 + b_1 \ln(t) \quad (3.4)$$

Cubic SPSS regression analysis expression

$$Y = b_0 + b_1 t + b_2 t^2 + b_3 t^3 \quad (3.5)$$

Power SPSS regression analysis expression

$$\ln(Y) = \ln(b_0) + b_1 \ln(t) \quad (3.6)$$

Using a MATLAB ‘polyfit’ function, we were able to get fit line expression equal to that of SPSS growth analysis. Therefore, in SPSS analysis we compared the three expressions. Figure 3.19 and 3.20 shows the SPSS regression analysis fit curves for the peaks and valley averaged values Table 3.2 shows the analysis resulting values. The closer R square is to 1, the better the fit of the equation.

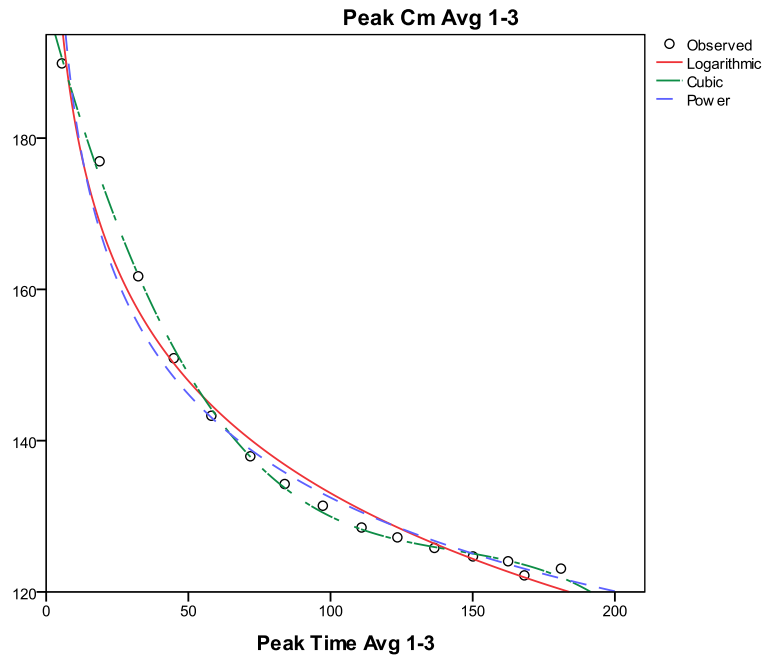


Figure 3.19 SPSS regression analysis curves for the average peaks.

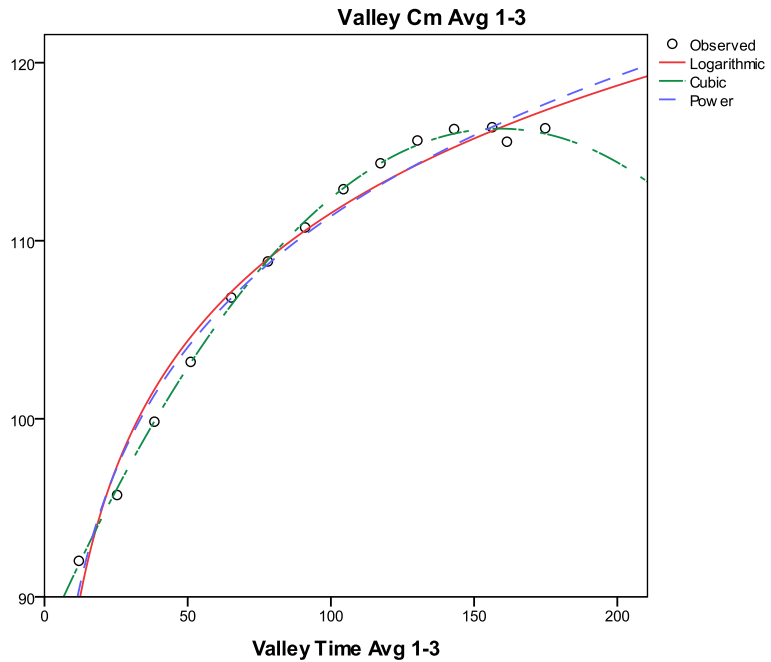


Figure 3.20 SPSS regression analysis curves for the average valleys.

Table 3.2 SPSS regression analysis results.

		R	R Square
Logarithmic	Peaks	0.988	0.976
	Valleys	0.988	0.976
Cubic	Peaks	0.999	0.998
	Valleys	0.999	0.999
Power	Peaks	0.985	0.970
	Valleys	0.990	0.980

From the SPSS regression analysis curves we see the logarithmic and power curves overlap each other and do not fit the data as well as the cubic curve. These

observations are supported by the trend of the  $R^2$  value being greatest for the cubic. At this time we will continue our analysis with the averaged peak and valley values as compared to the cubic analysis.

### 3.6.5 MATLAB analysis

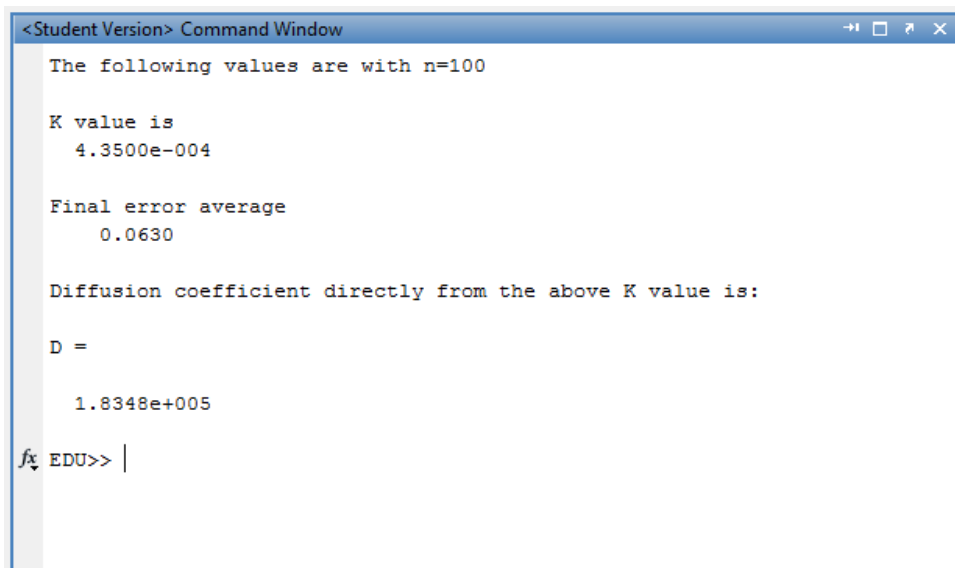
We developed a MATLAB program to solve for  $k$  and  $D$  using the SPSS regression cubic equation and the exponential part of equation (3.2). First, the program plots experimental averaged peaks and valleys. Next, using the regression analysis equation from SPSS, MATLAB calculates the concentration given the same time range and time steps as the experimental and plots the curve. Curve fit points at the same time as the experimental peaks are also plotted. Then, the MATLAB program has a while loop that compares the concentration from the SPSS equation and the concentration found for the theoretical equation for every time value given a guessed  $k$ . Since  $n$  still remains within the exponential part of the equation, there is a for loop within the while loop. This loop goes through the  $n$  values, 1 to 100, and summates the values with  $C_m$  and gives one  $C_{theoretical}$  value per time value. The loops create the following relationship.

$$C_{curve\ fit} = b_0 + b_1t + b_2t^2 + b_3t^3 = C_{theoretical} = C_m + \sum_{n=1}^{100} \left[ \exp\left(\frac{-4\pi^2}{L^2}kt\right) \right]^{n^2} \quad (3.7)$$

We set an error limit (a maximum) to 10%, once the error is reduced to that amount we are given a  $k$  value. Next, the program plots the theoretical concentration curve according to the determined  $k$  value. Also, the theoretical points at the same time

as the experimental peaks are plotted. Lastly, the diffusion coefficient was determined according to the equation (3.3) relationship.

Therefore, from our MATLAB program, we input a data set of averaged peaks and valley points per 3 tests, and SPSS cubic regression equation and its constants. Next, we get  $k$  and  $D$  values along with percent error between the concentrations calculated from the cubic regression equation and our diffusion equation using  $k$ . Figure 3.21 MATLAB output results and Figure 3.21 shows the graphic results for the concentration profile analyzing the data.



```
<Student Version> Command Window
The following values are with n=100

K value is
  4.3500e-004

Final error average
  0.0630

Diffusion coefficient directly from the above K value is:

D =

  1.8348e+005

fx EDU>> |
```

Figure 3.21 MATLAB output results of the peak value analysis of water and dye.

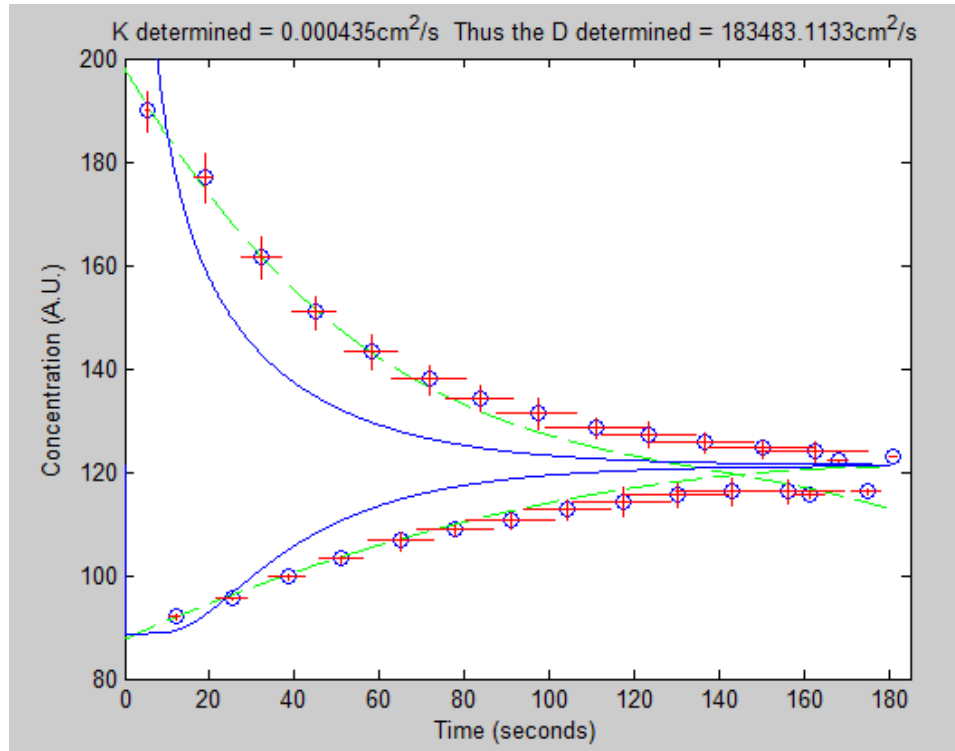


Figure 3.22 MATLAB plot of the peak value analysis of water and dye.

### 3.7 Conclusions

From Figure 3.22 the blue circles represent the average time and intensity values for the peak and valleys from test 1, 2, and 3. The red lines are the standard deviations of each point per intensity and time range values of the three tests. The two green dashed lines are the two cubic SPSS regression curves and while the two solid lines are the calculated curves using  $k$ . From the analysis performed on the water and dye experiments we get  $4.35 \times 10^{-4}$  cm<sup>2</sup>/s for  $k$  and  $1.838 \times 10^5$  cm<sup>2</sup>/s for  $D$  values. Using SPSS cubic regression analysis equation compared to our diffusion equation we calculated a 6.30% error in determining  $k$  and thus  $D$ . With all things considered, we assume our method is appropriate for determining an estimate of diffusion coefficient and has great potential in expediting the determination process.

We have developed a novel micro system device capable of experimentally mixing nanoliters of reagents together. By optically recording the movement and diffusion of the two reagents into one another we can obtain an intensity versus time curve. As the intensity is related to concentration, we can analyze the data to determine an experimental diffusion coefficient with the aid of SPSS and MATLAB analysis. By comparing the valley points versus the peak points from the data, after analysis the resulting dispersion and diffusion coefficients were within good agreement of each other.



## **Chapter 4**

### **Summary and conclusions**

#### **4.1 Conclusions of the research**

A progress of micro system device designs has been evaluated and tested. We were capable of developing a micro system device induced by micromixers within a series capable of experimentally mixing nanoliters of reagents together. We optically recorded and evaluated the resulting fluid flow of the two reagents mixing with one another. By improvement of baseline data analysis of the raw data, we were able to determine peak and valley points of the raw data and relate the change in each peak or valley by cubic regression analysis using SPSS software. We could determine an experimental diffusion coefficient using MATLAB analysis and part of an equation related to Fourier's concentration profile. By comparing the valley points versus the peak points from the data, after analysis the resulting dispersion and diffusion coefficients were within good agreement of water and dye solutions at 25.0 °. Further investigation can only improve the accuracy of the device and analysis process. We assume our method is appropriate for determining an estimate of diffusion coefficient and has great potential in expediting the determination process.

## References

1. Whitesides, G.M., *The origins and the future of microfluidics*. Nature, 2006. **442**(7101): p. 368-373.
2. Crank, J., *The mathematics of diffusion*. Second ed. 1975: Oxford University Press.
3. Culbertson, C.T., S.C. Jacobson, and J. Michael Ramsey, *Diffusion coefficient measurements in microfluidic devices*. Talanta, 2002. **56**(2): p. 365-373.
4. Terry, S.C., *A gas chromatography system fabricated on a silicon wafer using integrated circuit technology*. 1975.
5. Terry, S.C., J.H. Jerman, and J.B. Angell, *A gas chromatographic air analyzer fabricated on a silicon wafer*. Electron Devices, IEEE Transactions on, 1979. **26**(12): p. 1880-1886.
6. Reyes, D.R., et al., *Micro total analysis systems. 1. Introduction, theory, and technology*. Analytical chemistry, 2002. **74**(12): p. 2623-2636.
7. Manz, A., et al., *Design of an open-tubular column liquid chromatograph using silicon chip technology*. Sensors and Actuators B: Chemical, 1990. **1**(1-6): p. 249-255.
8. Manz, A., N. Graber, and H.M. Widmer, *Miniaturized total chemical analysis systems: a novel concept for chemical sensing*. Sensors and Actuators B: Chemical, 1990. **1**(1-6): p. 244-248.
9. Smits, J.G., *Piezoelectric micropump with three valves working peristaltically*. Sensors and Actuators A: Physical, 1990. **21**(1-3): p. 203-206.
10. Van de Pol, F.C.M., et al., *A thermopneumatic micropump based on micro-engineering techniques*. Sensors and Actuators A: Physical, 1990. **21**(1-3): p. 198-202.
11. Shoji, S., S. Nakagawa, and M. Esashi, *Micropump and sample-injector for integrated chemical analyzing systems*. Sensors and Actuators A: Physical, 1990. **21**(1-3): p. 189-192.
12. Esashi, M., *Integrated micro flow control systems*. Sensors and Actuators A: Physical, 1990. **21**(1-3): p. 161-167.
13. Northrup, M.A., et al., *Technical Digest of Transducers' 93: 7 th International Conference on Solid State Sensors and Actuators*. Yokohama, Japan, 1993: p. 924-927.
14. Hong, J.W. and S.R. Quake, *Integrated nanoliter systems*. Nature biotechnology, 2003. **21**(10): p. 1179-1183.
15. Weibel, D.B., et al., *Torque-actuated valves for microfluidics*. Analytical chemistry, 2005. **77**(15): p. 4726-4733.
16. Nguyen, N.T. and Z. Wu, *Micromixers—a review*. Journal of Micromechanics and Microengineering, 2005. **15**: p. R1.
17. Günther, A., et al., *Micromixing of miscible liquids in segmented gas-liquid flow*. Langmuir, 2005. **21**(4): p. 1547-1555.

18. Garstecki, P., M.A. Fischbach, and G.M. Whitesides, *Design for mixing using bubbles in branched microfluidic channels*. Applied Physics Letters, 2005. **86**: p. 244108.
19. Mrksich, M. and G.M. Whitesides, *Patterning self-assembled monolayers using microcontact printing: a new technology for biosensors?* Trends in biotechnology, 1995. **13**(6): p. 228-235.
20. Klaassen, E.H., et al., *Silicon fusion bonding and deep reactive ion etching: a new technology for microstructures*. Sensors and Actuators A: Physical, 1996. **52**(1-3): p. 132-139.
21. Zhao, X.M., Y. Xia, and G.M. Whitesides, *Fabrication of three dimensional micro structures: Microtransfer molding*. Advanced Materials, 1996. **8**(10): p. 837-840.
22. Zhao, X.M., Y. Xia, and G.M. Whitesides, *Soft lithographic methods for nano-fabrication*. J. Mater. Chem., 1997. **7**(7): p. 1069-1074.
23. Nguyen, N.T. and S.T. Wereley, *Fundamentals and applications of microfluidics*. 2002: Artech House Publishers.
24. Callister, W.D., *Materials Science and Engineering An Introduction*. 6th ed. 2003: John Wiley and Sons, Inc.
25. Unger, M.A., et al., *Monolithic microfabricated valves and pumps by multilayer soft lithography*. Science, 2000. **288**(5463): p. 113.
26. Chou, H.P., M.A. Unger, and S.R. Quake, *A microfabricated rotary pump*. Biomedical Microdevices, 2001. **3**(4): p. 323-330.
27. Cussler, E.L., *Multicomponent diffusion*. 1976: Elsevier.
28. Kreutzer, M.T., A. Günther, and K.F. Jensen, *Sample dispersion for segmented flow in microchannels with rectangular cross section*. Analytical chemistry, 2008. **80**(5): p. 1558.
29. Tyrrell, H.J.V. and K.R. Harris, *Diffusion in liquids, A theoretical and experimental study*. 1984.
30. Smeaton, W.A., *Berthollet's Essai de statique chimique and its translations: a bibliographical note and a Daltonian doubt*. Ambix, 1977. **24**(3): p. 149-158.
31. Fourier, J.B.J., *The analytical theory of heat*. 1878: The University Press.
32. Fick, A., *Ueber diffusion*. Annalen der Physik, 1855. **170**(1): p. 59-86.
33. Northrop, J.H. and M.L. Anson, *A METHOD FOR THE DETERMINATION OF DIFFUSION CONSTANTS AND THE CALCULATION OF THE RADIUS AND WEIGHT OF THE HEMOGLOBIN MOLECULE*. The Journal of General Physiology, 1929. **12**(4): p. 543-554.
34. Graham, T., *Liquid diffusion applied to analysis*. Philosophical Transactions of the Royal Society of London, 1861. **151**: p. 183-224.
35. Gouy, L.G., *Du pouvoir émissif des flammes colorées*. Comptes rendus, 1879. **88**: p. 418-421.
36. Taylor, G.I., *Diffusion and mass transport in tubes*. Proceedings of the Physical Society. Section B, 1954. **67**: p. 857-869.
37. Costin, C.D., et al., *Diffusion coefficient measurement in a microfluidic analyzer using dual-beam microscale-refractive index gradient detection:: Application to on-chip molecular size determination*. Journal of Chromatography A, 2003. **1013**(1-2): p. 77-91.

38. Xia, Y. and G.M. Whitesides, *SOFT LITHOGRAPHY*. Annual Review of Materials Science, 1998. **28**(1): p. 153-184.
39. Miyajima, H. and M. Mehregany, *High-aspect-ratio photolithography for MEMS applications*. Microelectromechanical Systems, Journal of, 1995. **4**(4): p. 220-229.
40. Pratt, K.C. and W.A. Wakeham, *The mutual diffusion coefficient of ethanol-water mixtures: determination by a rapid, new method*. Proceedings of the Royal Society of London. Series A, Mathematical and Physical Sciences, 1974. **336**(1606): p. 393-406.

## Appendix I

### MatLab Code

```
clear all
clc

Tp=xlsread('Data.xls','Data','A2:A20');%Peak averaged time
Cp=xlsread('Data.xls','Data','B2:B20');%Peak averaged concentration
Tv=xlsread('Data.xls','Data','C2:C20');%Valley averaged time(
Cv=xlsread('Data.xls','Data','D2:D20');%Valley averaged concentration
TsdP=xlsread('Data.xls','Data','E2:E20');%Peak standard deviation time
CsdP=xlsread('Data.xls','Data','F2:F20');%Peak standard deviation
concentration
TsdV=xlsread('Data.xls','Data','G2:G20');%Valley standard deviation
time
CsdV=xlsread('Data.xls','Data','H2:H20');%Valley standard deviation
concentration

Cpmax=max(Cp);%A.U.
L=0.7226;%cm
R=0.005;%cm
U=0.0674679;%cm/s
% Cm=108.5084;%Etest3 AU, light intensity
Cm=121.271;

disp('The following values are with n=100')
disp(' ')
plot(Tp,Cp,'o')%Plot full experimentatl data as a blue line
hold on
plot(Tv,Cv,'o')
hold on

bp0=198.004;
bp1=-1.393;
bp2=0.009;
bp3=-2.16E-05;
Tpc=0:0.1:180.5;
Cpc=bp0+bp1*Tpc+bp2*Tpc.^2+bp3*Tpc.^3;
plot(Tpc,Cpc,'--g')
hold on

bv0=87.631;
bv1=0.363;
bv2=-0.001;
bv3=8.71E-08;
Tvc=0:0.1:180.5;
Cvc=bv0+bv1*Tvc+bv2*Tvc.^2+bv3*Tvc.^3;
```

```

plot(Tvc,Cvc,'--g')
hold on

K=5e-4;%starting guess K
N = [1 2 3 4 5 6 7 8 9 10 11 12 13 14 15 16 17 18 19 20 21 22 23 24 25
26 27 28 29 30 31 32 33 34 35 36 37 38 39 40 41 42 43 44 45 46 47 48 49
50 51 52 53 54 55 56 57 58 59 60 61 62 63 64 65 66 67 68 69 70 71 72 73
74 75 76 77 78 79 80 81 82 83 84 85 86 87 88 89 90 91 92 93 94 95 96 97
98 99 100];
Tt = 0:0.1:180.5;

Cf=Cvc;
Ci=Cpc;
% Ct=Cf+190;
% avg_error_K = mean((Ct-Cf)./Cf);
avg_error_K=.3;
Ccal_sumv=Cm;
Ccal_sump=Cm;
%If the avg_error_K test value is too low, the loop will not stop
while avg_error_K >= 0.063
    K = K - 0.000001;

    for i = 1:length(N)
        n = N(i).^2;
        %for Minimum peaks Ccal = ((-exp(...
        Ccalv = ((-exp((-4.*(pi.^2).*K.*(Tt))./(L.^2))).^n);
        Ccal_sumv=Ccalv+Ccal_sumv;
        Ccalp = ((exp((-4.*(pi.^2).*K.*(Tt))./(L.^2))).^n);
        Ccal_sump=Ccalp+Ccal_sump;

    end

    errorKv=abs((Cf'-Ccal_sumv')./Cf');
    errorKi=abs((Ci'-Ccal_sump')./Ci');
    MeanKv = mean(errorKv);
    MeanKi = mean(errorKi);
    two=(MeanKv+MeanKi)/2;

    avg_error_K = mean(two);
    max_error_K = max(two);
    min_error_K = min(two);

end

disp('K value is')
disp (K)
disp('Final error average')
disp(avg_error_K)

Ctv=Ccal_sumv;
Ctp=Ccal_sump;

plot(Tt,Ctv,'b')
hold on
plot(Tt,Ctp,'b')
hold on

```

```

disp('Diffusion coefficient directly from the above K value is:')
D = ((48*K)/((R^2)*(U^2)))

xlabel('Time (seconds)')
ylabel('Concentration (A.U.)')
title(['K determined = ', num2str(K), 'cm^2/s', ' Thus the D determined = ', num2str(D), 'cm^2/s'])%manually change n value
% legend('Experimental', 'Experimental Peaks', 'Regression
Logarithmic', 'Regression Logarithmic Peaks', 'Theoretical', 'Theoretical
Peaks');
axis([0 185 80 200])
hold on

i=1:1:15;
A=[Tp(i)-TsdP(i), Tp(i), Tp(i)+TsdP(i)];
B=[Cp(i), Cp(i), Cp(i)];

x=A(1, :);
y=B(1, :);
plot(x,y, 'r')
hold on
x=A(2, :);
y=B(2, :);
plot(x,y, 'r')
hold on
x=A(3, :);
y=B(3, :);
plot(x,y, 'r')
hold on
x=A(4, :);
y=B(4, :);
plot(x,y, 'r')
hold on
x=A(5, :);
y=B(5, :);
plot(x,y, 'r')
hold on
x=A(6, :);
y=B(6, :);
plot(x,y, 'r')
hold on
x=A(7, :);
y=B(7, :);
plot(x,y, 'r')
hold on
x=A(8, :);
y=B(8, :);
plot(x,y, 'r')
hold on
x=A(9, :);
y=B(9, :);
plot(x,y, 'r')
hold on
x=A(10, :);
y=B(10, :);

```

```

plot(x,y,'r')
hold on
x=A(11,:);
y=B(11,:);
plot(x,y,'r')
hold on
x=A(12,:);
y=B(12,:);
plot(x,y,'r')
hold on
x=A(13,:);
y=B(13,:);
plot(x,y,'r')
hold on
x=A(14,:);
y=B(14,:);
plot(x,y,'r')
hold on
x=A(15,:);
y=B(15,:);
plot(x,y,'r')
hold on

i=1:1:15;
A=[Tp(i), Tp(i), Tp(i)];
B=[Cp(i)-CsdP(i), Cp(i), Cp(i)+CsdP(i)];

x=A(1,:);
y=B(1,:);
plot(x,y,'r')
hold on
x=A(2,:);
y=B(2,:);
plot(x,y,'r')
hold on
x=A(3,:);
y=B(3,:);
plot(x,y,'r')
hold on
x=A(4,:);
y=B(4,:);
plot(x,y,'r')
hold on
x=A(5,:);
y=B(5,:);
plot(x,y,'r')
hold on
x=A(6,:);
y=B(6,:);
plot(x,y,'r')
hold on
x=A(7,:);
y=B(7,:);
plot(x,y,'r')
hold on
x=A(8,:);

```



```

y=B(8,:);
plot(x,y,'r')
hold on
x=A(9,:);
y=B(9,:);
plot(x,y,'r')
hold on
x=A(10,:);
y=B(10,:);
plot(x,y,'r')
hold on
x=A(11,:);
y=B(11,:);
plot(x,y,'r')
hold on
x=A(12,:);
y=B(12,:);
plot(x,y,'r')
hold on
x=A(13,:);
y=B(13,:);
plot(x,y,'r')
hold on
x=A(14,:);
y=B(14,:);
plot(x,y,'r')
hold on
x=A(15,:);
y=B(15,:);
plot(x,y,'r')
hold on

i=1:1:14;
A=[Tv(i)-TsdV(i), Tv(i), Tv(i)+TsdV(i)];
B=[Cv(i), Cv(i), Cv(i)];

x=A(1,:);
y=B(1,:);
plot(x,y,'r')
hold on
x=A(2,:);
y=B(2,:);
plot(x,y,'r')
hold on
x=A(3,:);
y=B(3,:);
plot(x,y,'r')
hold on
x=A(4,:);
y=B(4,:);
plot(x,y,'r')
hold on
x=A(5,:);
y=B(5,:);
plot(x,y,'r')
hold on

```

```

x=A(6,:);
y=B(6,:);
plot(x,y,'r')
hold on
x=A(7,:);
y=B(7,:);
plot(x,y,'r')
hold on
x=A(8,:);
y=B(8,:);
plot(x,y,'r')
hold on
x=A(9,:);
y=B(9,:);
plot(x,y,'r')
hold on
x=A(10,:);
y=B(10,:);
plot(x,y,'r')
hold on
x=A(11,:);
y=B(11,:);
plot(x,y,'r')
hold on
x=A(12,:);
y=B(12,:);
plot(x,y,'r')
hold on
x=A(13,:);
y=B(13,:);
plot(x,y,'r')
hold on
x=A(14,:);
y=B(14,:);
plot(x,y,'r')
hold on

i=1:1:14;
A=[Tv(i), Tv(i), Tv(i)];
B=[Cv(i)-CsdV(i), Cv(i), Cv(i)+CsdV(i)];

x=A(1,:);
y=B(1,:);
plot(x,y,'r')
hold on
x=A(2,:);
y=B(2,:);
plot(x,y,'r')
hold on
x=A(3,:);
y=B(3,:);
plot(x,y,'r')
hold on
x=A(4,:);
y=B(4,:);
plot(x,y,'r')

```

```
hold on
x=A(5,:);
y=B(5,:);
plot(x,y,'r')
hold on
x=A(6,:);
y=B(6,:);
plot(x,y,'r')
hold on
x=A(7,:);
y=B(7,:);
plot(x,y,'r')
hold on
x=A(8,:);
y=B(8,:);
plot(x,y,'r')
hold on
x=A(9,:);
y=B(9,:);
plot(x,y,'r')
hold on
x=A(10,:);
y=B(10,:);
plot(x,y,'r')
hold on
x=A(11,:);
y=B(11,:);
plot(x,y,'r')
hold on
x=A(12,:);
y=B(12,:);
plot(x,y,'r')
hold on
x=A(13,:);
y=B(13,:);
plot(x,y,'r')
hold on
x=A(14,:);
y=B(14,:);
plot(x,y,'r')
hold on
```